

## Dynamical Models for Sea Floor Spreading

FRANK M. RICHTER

*Department of Earth and Planetary Sciences  
Massachusetts Institute of Technology  
Cambridge, Massachusetts 02139*

Fluid dynamic models of the lithosphere-asthenosphere system are studied. These models provide a basis for understanding driving mechanisms involved in sea floor spreading. The asthenosphere is represented as a highly viscous Newtonian fluid that is nonrotating, Boussinesq, incompressible, and nondissipative. A sequence of two-dimensional model problems is considered in an effort to understand the dynamic role of various energy sources available in the upper mantle. The first models investigate the role of vertical temperature gradients and find these incapable of generating flows in the asthenosphere that move overlying lithospheric plates by viscous traction. By considering the combined effect of horizontal and vertical temperature gradients, a mechanism for effecting the original breakup of large continental masses is suggested. The dynamic role of phase changes is investigated in a series of finite-amplitude model problems. The olivine-spinel phase transition is found to increase the amplitude of convection by a factor of about 2, and the depth at which the phase change occurs is influenced by the convection. A final class of problems explicitly consider the lithosphere coupled to the underlying asthenosphere and the mass flux into and out of the asthenosphere implied by moving surface plates. It is found that if the subducted lithosphere has a negative buoyancy of the order of present estimates, the lithospheric plates will move at velocities of 1-10 cm yr<sup>-1</sup>.

### CONTENTS

1. Introduction.....	224
2. Basic Assumptions and Simplifications.....	230
a. Newtonian Fluid.....	230
b. Boussinesq Approximation.....	232
c. Compressibility and Dissipation.....	233
d. Two-Dimensionality.....	234
e. Cartesian Coordinate System.....	235
f. Nonrotating System.....	235
3. Role of Vertical Temperature Gradients.....	236
4. Role of Horizontal Temperature Gradients.....	245
a. Modulated Convection.....	247
b. Horizontal Convection.....	252
c. Breakup Problem.....	254
5. Role of Phase Changes in the Asthenosphere.....	258
6. Lithosphere-Asthenosphere Models.....	270
a. Pacific Model.....	270
b. Atlantic Model.....	275

7. Conclusions.....	280
Appendix: Numerical Formulation of Model Problems.....	282
References.....	284

## 1. INTRODUCTION

Geology has always included concepts of a mobile, ever-changing surface of the earth. The presence of marine fossils, thousands of feet above sea level in highly folded mountain ranges, requires the acceptance of large-scale changes within continents. Nonetheless, a period of fierce controversy began when a meteorologist [Wegener, 1924] proposed that continents themselves were mobile and in fact that South America–Africa, once contiguous, had ‘drifted’ apart. This early notion of continental drift was inspired by the near parallelism of the Atlantic coasts of South America and Africa. The similarity of fossils older than 175 m.y. provided further evidence that in the past no barrier to the migration of species existed in what today is the Atlantic Ocean. The hostile reaction with which continental drift was received gave notice of the 50-year controversy to come.

The debate persisted so long for lack of new observations. It was not until the decade of the 1960's that new geophysical evidence strongly supported the idea that continents have changed and are now changing their spatial relationships.

*Vine and Matthews* [1963] were able to show that the elongated magnetic anomalies south of Iceland have a remarkable symmetry about the mid-Atlantic ridge; surveys over other portions of the mid-ocean ridge system revealed similar anomalies. If the sea floor were moving away from the mid-ocean ridges with new basaltic lavas emplaced to maintain a continuous crust, the new lavas would acquire a remanent magnetization in the direction of the geomagnetic field existing at the time of their formation. It is known that the earth's magnetic field undergoes periodic reversals of polarity and these reversals would thus “tag” a band of lavas formed during each polarity period. *Heirtzler et al.* [1968], using the accepted time scale of magnetic reversals and the elongated marine magnetic anomalies, were able to date the sea floor in the vicinity of the mid-ocean ridges. This dating allows for estimates of recent spreading velocities of the order of  $5 \text{ cm yr}^{-1}$ . A study of earthquakes with epicenters on the ridge axis [*Sykes*, 1967] indicates tensional fracturing and magmatic intrusion consistent with a spreading ocean floor. Continental drift had now become sea floor spreading.

The mid-ocean ridges, if considered ‘sources’ of new surface area, require the existence of equally strong ‘sinks’; such regions of surface area consumption are thought to exist in the island arc–deep sea trench areas of the world. Island arcs and deep sea trenches are the site of almost all deep earthquake activity and volcanism. *Oliver and Isacks* [1967], using earthquake data from the Tonga-Fiji trench, find a 100-km seismically anomalous zone dipping at approximately  $45^\circ$  and extending to a depth of almost 700 km under the trench. The zone is anomalous in that the attenuation of seismic waves is low and seismic

velocities are high relative to mantle material at similar depth elsewhere. The anomalous material is interpreted to be a subducted slab of surface material that maintains its physical integrity to depths in excess of 600 km. Similar anomalous zones are associated with almost all deep sea trenches, and therefore a sufficient system of sinks is proposed.

Geophysical interpretations leading to the concept of sea floor spreading at mid-ocean ridges and convergence at trenches can be integrated into a large-scale kinematic model of the earth, generally called the New Global Tectonics [*Isacks et al.*, 1968]. This model represents the surface of the earth as a finite number of 'plates' whose boundaries are outlined by seismically active areas (ridges and trenches). Figure 1 shows the plan form of the six largest plates [*Le Pichon*, 1968] superimposed on a map of earthquake epicenters for the period 1961–1967. The plates are assumed to be about 100 km thick and thus include both crust and uppermost mantle. Continents drift as a result of their being embedded in a moving plate. The plate material or lithosphere is considered to have 'significant strength,' which implies that it is relatively free of internal deformation as it moves from ridge to trench. The excellent 'fit' of the present coastlines of South America and Africa [*Bullard et al.*, 1965] are evidence of this strength. The plates must overlie a layer capable of fluidlike flow or creep that balances the mass flux implied by the plate motion. This layer, the asthenosphere, must extend to depths in excess of 600 km in the vicinity of the trenches to accommodate the subducted lithosphere. The nature of the return flow in the asthenosphere has not been determined by geophysical observations. Figure 2 is a simplified cross section from the Atlantic ridge to the East Pacific rise, which illustrates the main elements of the new global tectonic model.

Another class of geophysical observations, those of surface heat flow, also provides important evidence of the state of the crust and upper mantle. Most of the heat flowing to the surface of the earth today is due to energy released by the radioactive elements uranium, thorium, and potassium [*Simmons and Roy*, 1969]. These elements have been concentrated in the crust, especially in the thicker continental crust. The exact concentrations of radiogenic elements are not known, but some estimates indicate that continental crust contains up to 10 times more heat sources than oceanic crust. It is therefore surprising to find that globally averaged continental heat flow differs insignificantly from the mean oceanic value of  $1.5 \text{ cal cm}^{-2} \text{ sec}^{-1}$  [*Von Herzen and Lee*, 1969]. The classical interpretation of this observation is that the excess continental sources are compensated by a depletion at depth [*Bullard*, 1952]. *MacDonald* [1963] shows that for a static mantle the heat flow data and distribution of heat sources imply the existence of both vertical and horizontal temperature gradients. If one assumes that the asthenosphere is capable of fluidlike flow, there is a contradiction in using a static model for calculations of thermal structure, since horizontal gradients will always force motions that are capable of advecting heat. It must be kept in mind that the equality of heat flow holds only for global averages. Averages over areas of the order of  $10^5 \text{ km}^2$  can result in heat flow values that differ from the global mean by as much as a factor of 2 [*Simmons and Roy*, 1969; *Horai and Uyeda*, 1969].

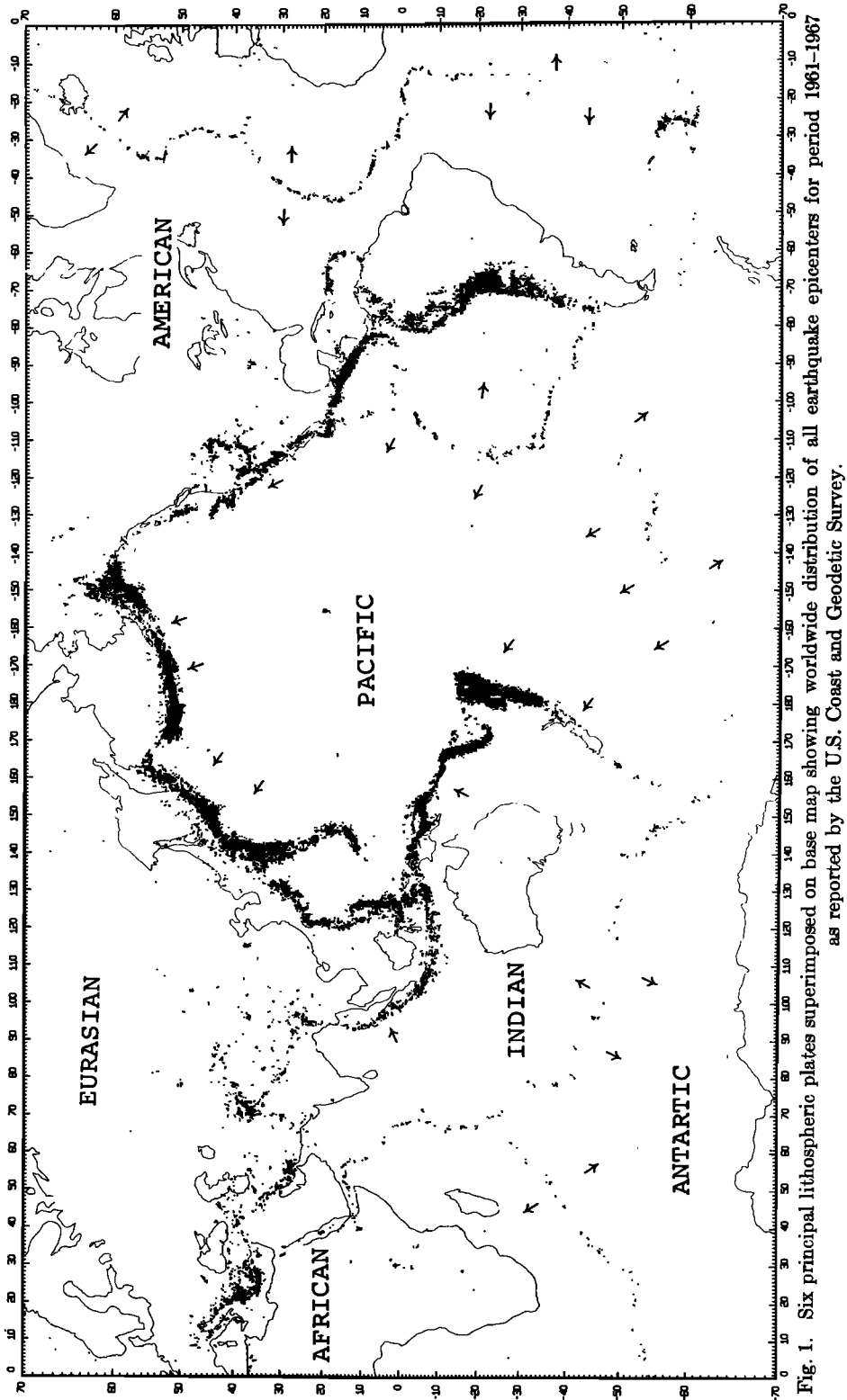


Fig. 1. Six principal lithospheric plates superimposed on base map showing worldwide distribution of all earthquake epicenters for period 1961-1967  
as reported by the U.S. Coast and Geodetic Survey.

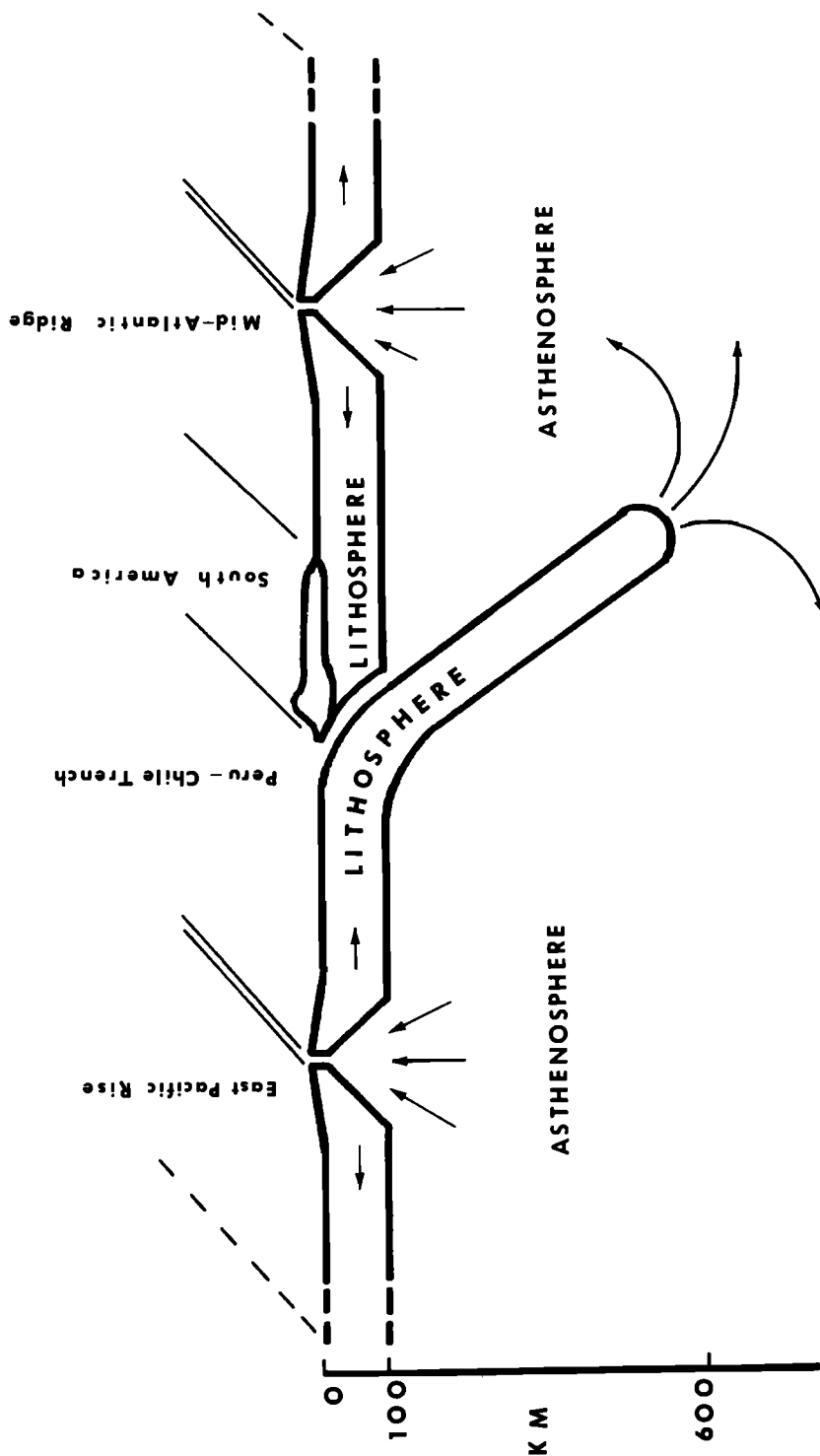


Fig. 2. Simplified cross section from East Pacific rise to Mid-Atlantic ridge.

The new global tectonics and the heat flow data give rise to many new questions as old ones are resolved. Two fundamental questions are (1) What is the nature of the flow in the asthenosphere implied by the moving lithospheric plates? and (2) What is the dynamics underlying the lithosphere-asthenosphere system? Furthermore, if the motions in the asthenosphere are capable of advecting significant heat, then these motions must be considered in any investigation of the earth's thermal structure.

Clearly there is need for new models of the earth that include mass transport below the lithosphere. Direct measurement of this transport does not seem feasible with present geophysical techniques because the velocities involved are of the order of centimeters per year. A presently viable approach is mathematical modeling of the lithosphere-asthenosphere system. Models would serve at least three principal purposes: (1) exploration of mechanisms capable of 'breaking up' large continental masses such as the once contiguous South America-Africa complex, (2) provision of a basis for understanding present-day motions and dynamics of the asthenosphere, and (3) relation of mass transport in the asthenosphere to some geophysically measurable property of the upper mantle.

The models considered are, in geologic terms, very oversimplified. This results from the limitations imposed by the formulation of tractable mathematical problems. Simplicity has its virtues. It leads to solutions that can be confirmed by alternate mathematical techniques or by comparing results with solutions of similar problems already in the literature. Such checks are especially important in the case of numerical solutions whose validity is often difficult to estimate a priori. In the case of complex models it may be impossible to effect checks that lead to confidence in the results. Furthermore, it may well be that, unless simpler models are first understood, complex cases will not be interpretable in terms of the contribution to the overall flow that each source of motion provides. It seems necessary, and perhaps even desirable, to consider relatively simple model problems at the outset.

It is well known that a horizontal layer of fluid heated from below becomes unstable and that convection cells appear when the vertical temperature gradient exceeds a critical value [Rayleigh, 1916]. The first group of models consider the asthenosphere driven by a supercritical temperature gradient. The geothermal gradient in the upper mantle may be supercritical [Knopoff, 1967], and it is important to understand the consequences of such a possibility.

The nonuniform distribution of radiogenic heat sources in the lithosphere suggests the existence of horizontal temperature gradients in the asthenosphere. The dynamic effect of these gradients is considered in a second series of model problems. The models investigate the role of horizontal gradients as a principal source of motion or as modifiers of flows driven primarily by unstable vertical gradients.

A third class of model problems considers the finite-amplitude effects of flow through a phase boundary. Phase changes are thought to occur at various depths in the mantle [Anderson, 1970; Ahrens and Syono, 1967; Birch, 1952], and it is of interest to ascertain their effect on motions driven by other energy sources.

A finite-amplitude theory would also relate vertical velocities to variations in the depth of the phase boundary. Such variations in depth may be detectable by seismic techniques and thus may provide an indirect method of estimating mass transport in the asthenosphere.

All the above models consider only the asthenosphere and do not include any explicit coupling to the lithosphere. Clearly, it is desirable to consider model problems that include the moving lithosphere and implied mass flux. A final class of model problems, their geometry motivated by Figure 2, consider the coupling of the two layers. These models include the effect of horizontal and vertical temperature gradients in conjunction with the subducted slab of lithospheric material, which is considered to be denser than the surrounding mantle [Turcotte and Schubert, 1971; Minear and Toksöz, 1970; McKenzie, 1969].

Many assumptions and simplifications, common to all model problems, are required to obtain a tractable set of governing equations. The degree of confidence with which certain terms can be neglected varies. In some cases, formal dimensional arguments clearly show that the neglect of a given term will not affect the basic balance of forces in the asthenosphere. Other assumptions are based on heuristic arguments and thus reflect varying degrees of a priori, subjective interpretation. The first section of this study is a statement of these assumptions and simplifications, and gives the basis on which they are made. This section is extremely important in that it defines the model equations and thus their limitations in representing the physical problem that motivates the model problems.

The later sections contain the formulation and solution of the model problems considered. The first group of models are driven solely by unstable vertical temperature gradients (Rayleigh-Benard convection) and are found to be inadequate as the cause of lithospheric motion. The main objections are (1) the stresses at the base of the lithosphere are periodic in space, with period smaller than typical plate dimensions, and therefore need not result in a net force away from a center of spreading; (2) the periodic nature of the flow does not allow for a net mass transport from trench to ridge in the asthenosphere; and (3) the time required by the cells to reach significant amplitude may be of the order of the age of the earth.

A second class of problems is considered in which the combined role of horizontal and vertical temperature gradients is investigated. Horizontal temperature gradients can modify the Rayleigh-Benard cells by modulating their amplitude and thus break the periodicity constraint. This alleviates the objection regarding the stresses on the base of the lithosphere. The analysis suggests that the combined effect of both horizontal and vertical temperature gradients may provide a mechanism for the breakup of large continental masses (South America-Africa), whereas the resulting smaller continents are stable to further breakup. These models do not satisfy the asthenosphere mass transport criteria and therefore must be modified once spreading has proceeded to the point of creating subduction zones.

The role of phase changes is next considered. The finite-amplitude model

presented in this study is in good agreement with the linear theory [Schubert and Turcotte, 1971] when sufficiently small amplitudes are considered. It is found that a phase change having the properties of the olivine-spinel transition is destabilizing and results in increased convective amplitude. The finite-amplitude theory also suggests that motions in the asthenosphere result in significant changes in the depth of the phase boundary, the changes being of the order of tens of kilometers.

A final class of problems considers both the asthenosphere and a moving lithosphere with the implied mass fluxes into (at trenches) and out of (at ridges) the asthenosphere. These models reflect the geometry of Figure 2. The principal conclusions from the coupled lithosphere-asthenosphere models are (1) convection resulting from horizontal and/or vertical temperature gradients is an inefficient mechanism for driving the lithospheric plates; and (2) if present estimates of the negative buoyancy of the downgoing slab are included as a driving mechanism, lithosphere velocities of the order of  $1-10 \text{ cm yr}^{-1}$  result.

The final section of this study summarizes the principal conclusions drawn from the model problems and relates them to geophysical and geologic observations. The most important conclusion is the primacy of the role of the downgoing lithospheric slabs and the mass flux they imply. It is found that the negative buoyancy of the slabs is the only mechanism among those considered that results in reasonable lithospheric velocities. Even if the negative buoyancy has been overestimated, the moving lithosphere and downgoing slabs impose velocity boundary conditions that cannot be ignored in the investigation of present day sea floor spreading dynamics.

The model problems suggest the following two-stage interpretation of the lithosphere-asthenosphere system. The original breakup of a large continental mass is effected by stresses generated by flows in the asthenosphere resulting from horizontal and vertical temperature gradients. This stage is relatively inefficient and may or may not result in significant spreading. Many continental-scale linear features may be records of frustrated spreading attempts. If the spreading exceeds a critical length, surface material is subducted and a new element is added to the dynamics, the negative buoyancy of the subducted material. This second stage is very efficient, and thus a period of rapid and irreversible spreading follows. The process is one of finite-amplitude instability of the lithosphere, in which the horizontal and vertical temperature gradients provide the finite perturbations.

## 2. BASIC ASSUMPTIONS AND SIMPLIFICATIONS

The assumptions and simplifications presented in this section, which result in a tractable set of governing equations, provide a basis for judging the relevance of the model problems considered in this study. One seeks to generate models sufficiently simple to be solvable but which retain the main elements of the dynamics of sea floor spreading.

a. *Newtonian fluid.* The appropriate constitutive equation relating the stress tensor to the rate of strain in the mantle is not known when long time

and space scales are considered. The simplest relationship is that of a Newtonian fluid in which the stress is a linear function of the rate of strain. Whether or not a material is Newtonian can only be established experimentally, since it is not possible to derive the constitutive relation from any macroscopic properties of the fluid.

Many authors [*Weertman, 1970; Berg, 1969; Orowan, 1965; Elsasser, 1963*] have suggested nonlinear relationships of stress versus rate of strain for the mantle. Such suggestions are in part motivated by experimental evidence that many materials are non-Newtonian at rates of strain as small as  $10^{-9}$  sec $^{-1}$ . Such rates of strain are still very rapid compared to estimates in the mantle of  $10^{-15}$  sec $^{-1}$  and thus do not necessarily imply a non-Newtonian mantle [*Run-corn, 1969*]. The exact constitutive relation appropriate for mantle materials may be very complex yet representable with sufficient accuracy by an apparent or equivalent Newtonian viscosity. The use of an apparent viscosity in geophysical problems is not without successful precedent. In the ocean the primary dissipation mechanism for large-scale flows is probably smaller-scale eddies. Nonetheless, the use of an apparent or eddy viscosity has been extremely useful in understanding the large-scale circulation.

Estimates of the apparent viscosity of the mantle are obtained from various sources. Using a uniform viscosity model, *Haskell [1935, 1936]* determined a mantle viscosity of  $10^{22}$  poises from the analysis of the isostatic rebound of Fennoscandia after the retreat of Pleistocene glaciers. A similar study of the rebound of Lake Bonneville, which drained on a very short time scale, determines a value of  $10^{21}$  poises [*Crittenden, 1963*]. The limited areal extent of these studies suggests that the results may be representative of only the uppermost mantle. *McConnell [1965, 1968]* and *Artyushkov [1967, 1971]* consider rebound data as a function of wavelength and, taking into account the non-hydrostatic shape of the earth, they determine viscosity as a function of depth. McConnell suggests that the value of  $10^{21}$  poises required by the rebound data is restricted to the uppermost mantle and that at greater depth viscosity increases to values of the order of  $10^{24}$  poises.

The use of the earth's nonhydrostatic equatorial bulge in conjunction with the tidal deceleration of the earth's rotation to determine mantle viscosity requires that the equatorial bulge be large compared to other departures from a hydrostatic shape. *Munk and MacDonald [1960a, b]* attribute the excess equatorial bulge to the long relaxation time of the earth's shape to rotational deceleration. Such an explanation results in a mantle viscosity of  $7.9 \times 10^{25}$  poises [*MacDonald, 1966*]. *Goldreich and Toomre [1969]* have subsequently shown that the equatorial bulge is not anomalously large compared to other nonhydrostatic components of the earth's shape and thus seriously question the interpretation of Munk and MacDonald.

*Dicke [1966, 1969]* and *O'Connell [1971]* use an entirely different approach. They use historical eclipse data to obtain high-precision information about the nontidal changes in the earth's rotation. This change in rate of rotation is interpreted as arising from changes in the earth's moment of inertia, which result from the noninstantaneous isostatic adjustment of ocean basins to Pleistocene

glacier melt water. The time scale of ocean basin adjustment suggests a uniform mantle viscosity of the order of  $10^{22}$  poises.

For the present study the viscosity is assumed to be Newtonian and uniform over the domain of calculation. This choice ignores changes with depth and also any possible coupling of the viscosity to the temperature field. The nonlinear coupling of viscosity to temperature in a fluid is an exceedingly difficult mathematical problem and represents a major area of study in itself [Torrance and Turcotte, 1971]. The choice of a uniform Newtonian viscosity is justified in an operational sense; it leads to tractable model equations, which may or may not have to be modified as the understanding of the rheological state of the mantle increases. Again, an analogy with the development of oceanography guides the approach used in this study. The ocean is a stratified fluid. Despite their obvious limitations, early homogeneous ocean models resulted in a quantum increase in the understanding of oceanic circulation and also provided the basis for more sophisticated models. In a similar sense, the uniform viscosity problems are at worst a necessary first step in the development of more complex models of the asthenosphere.

The role of the thermometric conductivity of a material is similar to that of viscosity in that it determines the structure of the governing equations and measures the rate of diffusion. In this study the coefficient of thermometric conductivity  $\kappa$  is considered uniform. Again, formal arguments supporting this choice are not possible, and one is guided by the same philosophy that was used in assuming a uniform viscosity. A recent experimental study of the total thermal conductivity (lattice plus radiative) of several important earth materials in the temperature range  $500^{\circ}\text{--}1900^{\circ}\text{K}$  results in estimates of a relatively constant  $\kappa$  of the order of  $10^{-2} \text{ cm}^2 \text{ sec}^{-1}$  [Schatz and Simmons, 1972]. Turcotte and Oxburgh [1972] give a review of the behavior of  $\kappa$  in the mantle and suggest a similar value.

b. *Boussinesq approximation.* The Boussinesq approximation involves the neglect of variations in density from a constant value in all terms of the equations of motion except when the density variations are multiplied by gravity (the buoyancy term). The approximation is justified if the variations are small compared with the mean density of the fluid.

The dynamically important variations in density, aside from the effect of phase changes, can be written as a function of the temperature alone:

$$\rho = \rho_0[1 + \alpha(T_0 - T)]$$

where

$\alpha$  coefficient of expansion.

$T$  temperature.

$\rho_0$  density at reference temperature  $T_0$ .

We do not mean to imply by this equation of state that density does not increase with depth. The effect of pressure on density is ignored in that it does not enter the dynamics of the system. In order that  $\rho_0$  replace  $\rho$  in all terms except the

buoyancy term, it is required that  $\alpha (T_0 - T) \ll 1$ . Using  $\alpha = 4 \times 10^{-5} \text{C}^{-1}$  [McKenzie, 1969] and a maximum temperature variation of  $1000^\circ\text{C}$  gives

$$\alpha(T_0 - T) \leq 4 \times 10^{-2}$$

which is sufficient to justify the Boussinesq approximation.

c. *Compressibility and dissipation.* The velocity in the asthenosphere is sufficiently small so that the pressure can be considered hydrostatic, and thus the change in entropy can be written:

$$ds = C_p dT/T + g\alpha dz$$

and the thermodynamic equation becomes

$$\partial T/\partial t + u \partial T/\partial x + w(\partial T/\partial z + g\alpha T/C_p) = \kappa \nabla^2 T + H/\rho C_p + \Phi/\rho C_p$$

where

$C_p$  specific heat at constant pressure.

$g$  gravity.

$\kappa$  thermometric conductivity, assumed constant.

$H$  heat added by radiogenic sources.

$\Phi$  heat added by viscous dissipation.

$g\alpha T/C_p$  adiabatic lapse rate.

and where  $\alpha$  is the coefficient of expansion, and the Z-axis points upward. The viscous dissipation  $\Phi$  is order  $(\mu U^2/D^2)$ , where

$\mu$  viscosity coefficient.

$U$  typical velocity scale.

$D$  typical length scale.

The importance of the dissipation term can be estimated by the ratio of the dissipation term and the thermal diffusion term:

$$\frac{\text{Dissipation}}{\text{Diffusion}} \approx \frac{(\mu/\rho C_p)(U^2/D^2)}{(\kappa \Delta T/D^2)} = \frac{\nu U^2}{C_p \kappa \Delta T}$$

where

$\nu$  the kinematic viscosity;  $\nu = \mu/\rho$ .

$\Delta T$  typical temperature scale.

The parameters are not known exactly, but the ratio may be as large as order 1. This indicates that the role of dissipation is not negligible, especially in models driven primarily by temperature gradients. Despite this estimate, the heat of dissipation will be neglected in the thermodynamic equation. At a later date it can be added to models of particular geophysical interest. In the case of models not driven primarily by thermal gradients, the neglect of dissipation should have little effect on the velocity field. Nonetheless, even in these cases it would be interesting to include dissipation, since it will provide local heating at the base of the lithosphere, which may help explain the distribution of volcanism.

One can similarly estimate the importance of compressibility by considering the ratio of the adiabatic gradient to the total vertical temperature gradient:

$$\frac{\text{Compressibility}}{\text{Vertical gradient}} = \frac{g\alpha T/C_p}{\partial T/\partial z} \approx \frac{10^3 \times 4 \times 10^{-5} \times 10^3 \times 10^{-7}}{10^3/5 \times 10^7} = 0.2$$

when the depth is assumed to be about 500 km.

This estimate indicates that to a first approximation the effect of compressibility can be ignored. This is true if one considers that the dynamically important quantity is the difference between the geothermal and adiabatic temperature gradients, and it is redundant to include the adiabatic gradient when the geothermal gradient is not well known. Figure 3 shows the adiabatic geotherm [Verhoogen, 1951] and a calculated geothermal gradient for a non-convecting earth of chondritic composition [MacDonald, 1963]. This figure supports the contention that the effect of compressibility is small compared with a reasonable vertical temperature scale.

*d. Two-dimensionality.* All models considered are two-dimensional. In terms of the dynamics of sea floor spreading, the most important components of asthenosphere velocity lie in the same plane as the spreading and subduction velocity vectors of the lithosphere. It is these components that must balance the mass flux implied by the moving lithosphere and must also control the overall dynamic influence of the asthenosphere on the lithosphere. For this reason, and because the system can be considered nonrotating (as will be seen), two-dimensional models will be capable of resolving the basic dynamics of the

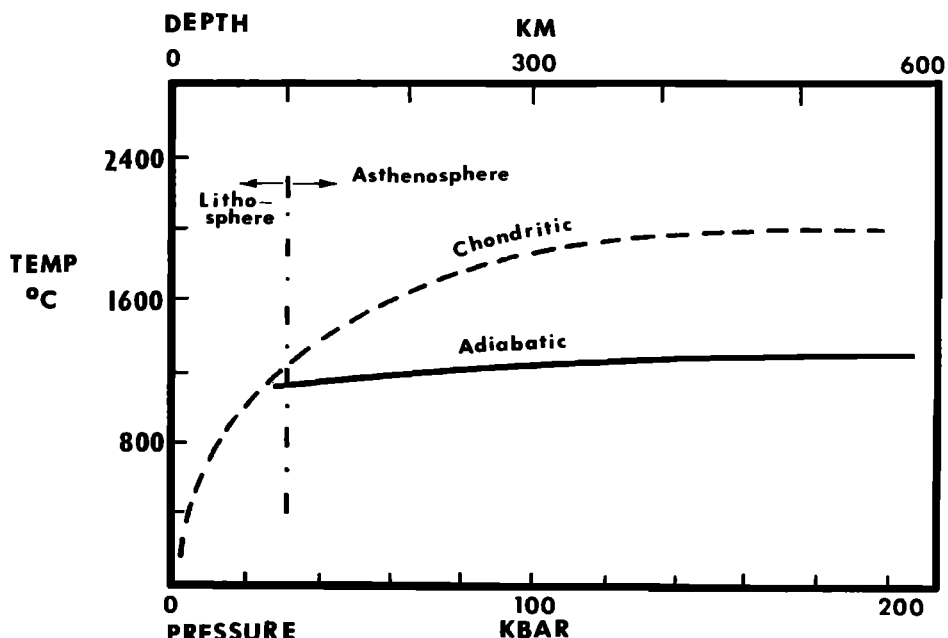


Fig. 3. Adiabatic [after Verhoogen, 1951] and chondritic [after MacDonald, 1963] temperature gradients.

lithosphere-asthenosphere system. The implied restriction that cellular convection be in the form of two-dimensional rolls is consistent with the assumption that the properties of the fluid are uniform.

e. *Cartesian coordinate system.* The natural coordinate system for the mantle is spherical, but a Cartesian coordinate system is easier. In order to ignore sphericity one must require that

$$D/R \ll 1 \quad \frac{\cos \phi_0}{\cos \phi} \approx 1$$

where

- D* depth of fluid.
- R* radius of the earth.
- ϕ* latitude of any point in domain.
- ϕ<sub>0</sub>* reference latitude within domain.

If the depths considered do not greatly exceed 1000 km, the first constraint is at least weakly satisfied. The second requirement, although not formally satisfied, will result only in geometric distortions that do not affect the balance of forces in the system.

f. *Nonrotating system.* The relative importance of the Coriolis force can be estimated by comparing it with the viscous term in the momentum equation.

$$\frac{\text{viscous}}{\text{Coriolis}} = \frac{\nu U/D^2}{2\Omega U} = \frac{\nu}{2\Omega D^2} = \text{Ekman number} = E$$

where  $2\Omega$  is twice the earth's angular velocity, and  $D$  is the typical length scale. Even if distances of the order of 10,000 km are considered, the Ekman number is  $10^7$ . Further confirmation of the insignificance of rotation in mantle problems comes from considering the effect of rotation on Rayleigh-Benard convection. For rotation to have any effect on convection, the Taylor number ( $4\Omega^2 D^4 / \nu^2$ ) must be greater than order 1 [Chandrasekhar, 1961]. We find that

$$\text{Taylor number} = 1/E^2 \approx 10^{-14}$$

Clearly, the neglect of rotation is the best of the simplifications required for this study.

The fluid-dynamic equations in Cartesian coordinates governing a system that is (1) Newtonian, (2) Boussinesq, (3) incompressible and nondissipative, (4) two-dimensional, and (5) non-rotating are

The momentum equation

$$D\mathbf{q}/Dt = 1/\rho_0 \nabla p + \nu \nabla^2 \mathbf{q} - g\alpha(T_0 - T)\hat{k} \quad (1)$$

where

- $\mathbf{q}$  velocity vector;  $\mathbf{q} = u\hat{i} + w\hat{k}$ .
- $p$  pressure.
- $\nu$  kinematic viscosity.

and where  $\rho_0$  is density at reference temperature  $T_0$ ,  $T$  is temperature,  $g$  is gravity,  $\alpha$  is the coefficient of thermal expansion, and

$$\begin{aligned} D/Dt &= \partial/\partial t + \mathbf{q} \cdot \nabla \\ \nabla &= \partial/\partial x\hat{i} + \partial/\partial z\hat{k} \\ \nabla^2 &= \partial^2/\partial x^2 + \partial^2/\partial z^2 \end{aligned}$$

The continuity equation

$$\nabla \cdot \mathbf{q} = 0 \quad (2)$$

The thermal equation

$$DT/Dt = \kappa \nabla^2 T + H/\rho_0 C_p \quad (3)$$

where  $\kappa$  is thermometric conductivity,  $C_p$  is specific heat, and  $H$  represents radiogenic heat sources.

The equation of state

$$\rho = \rho_0[1 + \alpha(T_0 - T)] \quad (4)$$

For a more detailed discussion of equations 1–4, see *Chandrasekhar* [1961] and *McKenzie* [1968].

### 3. ROLE OF VERTICAL TEMPERATURE GRADIENTS

Both mathematical solutions and experimental evidence indicate that a fluid layer heated from below is quiescent until the heat flow exceeds a critical value, at which time cellular convection begins. Such cellular motions (Rayleigh-Bénard convection) have long been contemplated as a possible driving mechanism of the surface plates [*Holmes*, 1928]. More recent studies [*Torrance and Turcotte*, 1971] have attempted to provide a formal basis for the general concept that sea floor spreading is driven by the energy stored in unstable vertical temperature gradients. It is therefore appropriate to begin the systematic search for viable mechanisms by considering Rayleigh-Bénard convection.

Finite-amplitude solutions for a fluid layer heated from below can be obtained analytically [*Malkus and Veronis*, 1958; *Kuo*, 1961]. A simple finite-amplitude theory, similar in most respects to that of *Malkus* and *Veronis*, is reviewed; the theory illustrates some of the characteristics of Rayleigh-Bénard convection. This development also defines the notation and the nondimensionalization used throughout this study.

Consider the problem of a horizontally infinite layer of fluid heated from below, as shown in Figure 4. The equations governing the system are (1–4) of the previous section. These equations are nondimensionalized by

$$\begin{pmatrix} x \\ z \end{pmatrix} = D \begin{pmatrix} x' \\ z' \end{pmatrix}$$

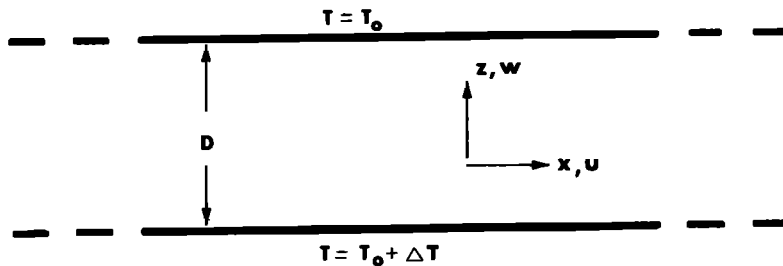


Fig. 4. Rayleigh-Benard convection model.

$$\begin{pmatrix} u \\ w \end{pmatrix} = \kappa/D \begin{pmatrix} u' \\ w' \end{pmatrix}$$

$$T = T_0 + \Delta T \theta'$$

$$P = P_{\infty} - \rho_0 g D Z' + \rho_0 (\kappa/D)^2 p'$$

where  $\Delta T$  is the temperature difference between  $z' = 0$  and  $z' = 1$ ,  $P_{\infty}$  is an arbitrary constant, and  $\rho_0$  is the density at  $T = T_0$ .

If a supercritical layer of fluid is randomly perturbed, then once Rayleigh-Benard convection reaches small but finite amplitude, the subsequent time evolution involves only a monotonic growth of the amplitude to its steady state value, with no changes in the geometry of the flow. For this reason, steady solutions are an accurate description of the geometry of the flow during the period of growth; they also provide a measure of the final equilibrated amplitude. This suggests that steady solutions are sufficient to illustrate several serious objections to Rayleigh-Benard convection as the primary mechanism driving sea floor spreading. Thus, for the moment we shall consider the steady problem and shall discuss the time scale for the evolution of the amplitude separately. The dimensionless equations, after dropping primes, become

$$\mathbf{q} \cdot \nabla \mathbf{q} = - \nabla p + \sigma \nabla^2 \mathbf{q} + \sigma R_a \theta \hat{k} \quad (5)$$

$$\mathbf{q} \cdot \nabla \theta = \nabla^2 \theta \quad (6)$$

$$\nabla \cdot \mathbf{q} = 0 \quad (7)$$

where

$$\sigma = \nu/\kappa \quad \text{the Prandtl number}$$

$$R_a = \frac{g \alpha \Delta T D^3}{\kappa \nu} \quad \text{the Rayleigh number}$$

A final simplification is made in the choice of the dynamic boundary condition. Clearly, the vertical velocity must vanish at  $z = 0$  and  $z = 1$ . Rather than consider  $u = 0$  on horizontal boundaries (no-slip condition), following Rayleigh, we shall require that  $\partial u / \partial z = 0$  on  $z = 0$  and  $z = 1$ . This no-stress or "free" boundary condition simplifies the analysis without significantly changing the results. The complete boundary conditions are

$$w = w_{zz} = 0 \quad \theta = 0 \quad \text{at} \quad z = 1$$

(subscripts  $x$  or  $z$  denote partial differentiation) and

$$w = w_{zz} = 0 \quad \theta = 1 \quad \text{at} \quad z = 0$$

The boundary condition on  $u$  has been transformed into a condition on  $w$  by using the continuity equation 7.

The nonlinear terms in (5) and (6) require that the analysis be restricted to small amplitudes in order that the nonlinearities can be ignored to the lowest order in some small parameter  $\epsilon$ , which is a measure of the amplitude. Let  $\epsilon = (R_a - R_c)^{1/2}/R_c$ , where  $R_c$  is the critical Rayleigh number, which will be determined by the analysis. The dependent variables can be expanded in an asymptotic series in  $\epsilon$ :

$$\mathbf{q} = \mathbf{q}_0 + \epsilon \mathbf{q}_1 + \epsilon^2 \mathbf{q}_2 + \epsilon^3 \mathbf{q}_3 + \dots \quad (8a)$$

$$\theta = \theta_0 + \epsilon \theta_1 + \epsilon^2 \theta_2 + \dots \quad (8b)$$

$$p = p_0 + \epsilon p_1 + \epsilon^2 p_2 + \dots \quad (8c)$$

and, from the definition of  $\epsilon$ ,

$$R_a = R_c + \epsilon^2 R_c \quad (8d)$$

Substitution of (8) into (5) through (7) results in a lowest-order problem:

$$\mathbf{q}_0 \cdot \nabla \mathbf{q}_0 = -\nabla p_0 + \sigma \nabla^2 \mathbf{q}_0 + \sigma R_c \theta_0 \hat{k} \quad (9a)$$

$$\mathbf{q}_0 \cdot \nabla \theta_0 = \nabla^2 \theta_0 \quad (9b)$$

$$\nabla \cdot \mathbf{q}_0 = 0 \quad (9c)$$

The boundary conditions at this order are

$$w_0 = w_{0zz} = \theta_0 = 0 \quad z = 1$$

$$w_0 = w_{0zz} = 0, \theta_0 = 1 \quad z = 0$$

The solution  $\mathbf{q}_0 = 0, \theta_0 = (1 - z)$  satisfies all boundary conditions and represents a purely conductive state. It is this state of quiescence whose stability we proceed to investigate. The order  $\epsilon$  problem is governed by

$$0 = -\nabla_{p_1} + \sigma \nabla^2 \mathbf{q}_1 + \sigma R_c \theta_1 \hat{k} \quad (10a)$$

$$w_1 \partial \theta_0 / \partial z = \nabla^2 \theta_1 \quad (10b)$$

$$\nabla \cdot \mathbf{q}_1 = 0 \quad (10c)$$

The boundary conditions at this order are

$$w_1 = w_{1zz} = \theta_1 = 0 \quad z = 0, 1$$

By using the operator  $\hat{k} \cdot \nabla \times \nabla \times$  on equation 10a,  $u_1$  and  $p_1$  are eliminated:

$$\hat{k} \cdot \nabla \times \nabla \times (-\nabla p_1 + \sigma \nabla^2 \mathbf{q}_1 + \sigma R_c \theta_1 \hat{k}) = -\sigma R_c \frac{\partial^2 \theta_1}{\partial x^2} - \sigma \nabla^4 w_1 = 0 \quad (11)$$

If we eliminate  $\theta_1$  between (11) and (10b),

$$\mathcal{L}(w_1) = \sigma \nabla^6 w_1 - \sigma R_c \frac{\partial^2}{\partial x^2} w_1 / \partial x^2 = 0 \quad (12)$$

This equation has a solution,

$$w_1 = (A \cos mx + B \sin mx) \sin n\pi z \quad (13)$$

where  $A$  and  $B$  are constants, provided that

$$R_c = (m^2 + n^2\pi^2)^3/m^2$$

which defines a neutral curve of  $R_c$  versus  $m$  for each  $n$  such that the fluid is stable for  $R_a < R_c$  and unstable if  $R_a > R_c$ . The most unstable mode corresponds to  $n = 1$ ,  $m = m_c = \pi/(2)^{1/2}$ , for which  $R_c = 657.5$ .

Using equations 10c and 11, we obtain  $u_1$  and  $\theta_1$  from  $w_1$ :

$$u_1 = -(\pi/m)(A \sin mx - B \cos mx) \cos \pi z \quad (14)$$

$$\theta_1 = [1/(m^2 + \pi^2)](A \cos mx + B \sin mx) \sin \pi z \quad (15)$$

The order  $\epsilon$  problem resolves the structure of the flow when  $R_a > R_c$  but does not determine the amplitude coefficients  $A$  and  $B$ . The amplitude is obtained by considering higher order in  $\epsilon$ .

Using the operator  $\hat{k} \cdot \nabla \times \nabla \times$  on the  $\epsilon^2$  momentum equation, we find

$$\sigma \nabla^4 w_2 + \sigma R_c \frac{\partial^2 \theta_2}{\partial x^2} = \frac{\partial^2}{\partial x^2} (\mathbf{q}_1 \cdot \nabla w_1) - \frac{\partial^2}{\partial x \partial z} (\mathbf{q}_1 \cdot \nabla u_1) - \sigma R_c \frac{\partial^2 \theta_0}{\partial x^2} \quad (16)$$

The remaining equations at order  $\epsilon^2$  are

$$\mathbf{q}_1 \cdot \nabla \theta_1 + w_2 \frac{\partial \theta_0}{\partial z} = \nabla^2 \theta_2 \quad (17a)$$

$$\nabla \cdot \mathbf{q}_2 = 0 \quad (17b)$$

with boundary conditions

$$w_2 = w_{2,..} = \theta_2 = 0 \quad z = 0, 1$$

It should be noted that the nonlinear terms in (16) and (17a) are products of lower-order solutions and thus are already determined. The asymptotic expansion of the dependent variables has reduced the nonlinear equations to a tractable set of linear equations.

Evaluating the nonlinear terms, we find that (16) and (17) become

$$\sigma \nabla^4 w_2 + \sigma R_c \frac{\partial^2}{\partial x^2} \theta_2 = 0 \quad (18a)$$

$$\nabla^2 \theta_2 + w_2 = [\pi/(m^2 + \pi^2)](A^2 + B^2) \sin \pi z \cos \pi z \quad (18b)$$

$$\nabla \cdot \mathbf{q}_2 = 0 \quad (18c)$$

Eliminating  $\theta_2$  between (18a) and (18b) gives

$$\mathcal{L}(w_2) = 0 \quad (19)$$

with  $\mathcal{L}$  as in (12).

The equation and boundary conditions for  $w_2$  are identical to those governing  $w_1$  (see equation 12), and thus we can choose  $w_2 = 0$  without loss of generality. This is equivalent to a normalization condition requiring that all solutions to the completely homogeneous problem for  $w$  be included in  $w_1$ . The complete solution to order  $\epsilon^2$  is

$$w_2 = 0 \quad (20a)$$

$$u_2 = 0 \quad (20b)$$

$$\theta_2 = -\frac{(A^2 + B^2)}{8\pi(m^2 + \pi^2)} \sin 2\pi z \quad (20c)$$

The constants  $A$  and  $B$  are still unresolved, and one must again proceed to the next order in  $\epsilon$ . The  $\epsilon^3$  equations are

$$\begin{aligned} \sigma \nabla^4 w_3 + \sigma R_c \frac{\partial^2 \theta_3}{\partial x^2} &= \frac{\partial^2}{\partial x^2} (\mathbf{q}_1 \cdot \nabla w_2) - \frac{\partial^2}{\partial x \partial z} (\mathbf{q}_1 \cdot \nabla U_2) \\ &\quad + \frac{\partial^2}{\partial x^2} (\mathbf{q}_2 \cdot \nabla w_1) - \frac{\partial^2}{\partial x \partial z} (\mathbf{q}_2 \cdot \nabla U_1) - \sigma R_c \frac{\partial^2 \theta_1}{\partial x^2} \end{aligned} \quad (21a)$$

$$\nabla^2 \theta_3 - w_3 \frac{\partial \theta_0}{\partial z} = u_1 \frac{\partial \theta_2}{\partial x} + u_2 \frac{\partial \theta_1}{\partial x} + w_1 \frac{\partial \theta_2}{\partial z} + w_2 \frac{\partial \theta_1}{\partial z} \quad (21b)$$

$$\nabla \cdot \mathbf{q}_3 = 0 \quad (21c)$$

with boundary conditions  $w_3 = w_{3..} = \theta_3 = 0$  at  $z = 0, 1$ . Evaluating the nonlinear terms on the right-hand side and eliminating  $\theta_3$  between (21a) and (21b), we can state the problem in terms of  $w_3$  alone:

$$\begin{aligned} \mathcal{L}(w_3) &= -\sigma(m^2 + \pi^2)^3(A \cos mx + B \sin mx) \sin \pi z \\ &\quad + [\sigma/8(m^2 + \pi^2)^2](A^2 + B^2)(A \cos mx + B \sin mx)(\sin \pi z - \sin 3\pi z) \end{aligned} \quad (22)$$

The inhomogeneous terms proportional to  $(\sin mx \sin \pi z)$  and  $(\cos mx \sin \pi z)$  are solutions of the homogeneous problem satisfying the boundary conditions. These terms, if not constrained, will give rise to a secular term (in  $x$ ), rendering our original expansion of  $w$  invalid. The necessary constraint determines the amplitude of the convective cells. The secularity is removed if

$$[(m^2 + \pi^2)^2/8](A^2 + B^2) - (m^2 + \pi^2)^3 = 0 \quad (23a)$$

or

$$A^2 + B^2 = 8(m^2 + \pi^2) \quad (23b)$$

At this point it is convenient to redefine the amplitude coefficients. Let

$$Re^{i\phi} = A + iB \quad (24)$$

In this notation the order  $\epsilon$  solution (13) becomes

$$w_1 = Re [Re^{i(mz+\phi)}] \sin \pi z \quad (25)$$

where  $R$  is the amplitude and  $\phi$  is the phase of the order  $\epsilon$  solution.

The amplitude equation 23b becomes simply

$$R = [8(m^2 + \pi^2)]^{1/2} = 10.88 \quad [m = m_c = \pi/(2)^{1/2}] \quad (26)$$

and  $\phi$  is an undetermined constant. The finite-amplitude solution for  $w$  is

$$w = \epsilon \operatorname{Re} \{10.88 \exp[i(m_c x + \phi)]\} \sin \pi z + O(\epsilon^2) \quad (27)$$

The order  $\epsilon^3$  problem thus determines the amplitude of the cellular convection whose structure is defined by the order  $\epsilon$  problem. The undetermined phase  $\phi$  of the solution just means that a horizontally infinite layer of fluid has no mechanism that determines where the cells reside in  $x$  space.

Had we not restricted our attention to the steady solution, time would have been nondimensionalized by

$$t = (D^2/\kappa)t'$$

The amplitude is found to develop on a slow  $O(\epsilon^2)$  time scale [Segel, 1969], and the resulting amplitude equation is

$$(dR/d\tau)(\tau) = R_{(\tau)} - R_{(\tau)}^3 [8(m^2 + \pi^2)]^{-1} \quad (28)$$

where

$$\tau = (m^2 + \pi^2)\epsilon^2[\sigma/(1 + \sigma)]t' \quad (29)$$

The time scale depends on the amplitude of the motion, and Knopoff [1969] has argued that velocities of the order of centimeters per year imply a "growth" time of the order of 1 b.y.

The solution (27) cannot be valid for all  $\epsilon$ . An important question is for what range of  $\epsilon$  is (27), which represents steady, two-dimensional rolls, valid. If  $\epsilon$  is vanishingly small, the fluid is not truly Boussinesq, and the plan form is hexagonal rather than in the form of rolls (Benard convection). For finite values of  $\epsilon$ , experiments [Krishnamurti, 1970a, b] indicate that two-dimensional rolls are the preferred form of convection if  $\epsilon^2 < 12$  and  $\sigma > 1$ . For  $\epsilon^2 > 12$ , the flow becomes first three-dimensional and finally time dependent. Furthermore, a theoretical solution by Kuo [1961] indicates that a single-mode analysis, which ignores all higher harmonics, is valid up to  $\epsilon = 1$ . Thus solution (27) is valid for  $\epsilon$  slightly greater than 0 and less than or equal to 1.

Solutions in the range  $1 < \epsilon^2 < 12$  can be obtained by a two-dimensional finite difference analysis. A numerical model that accepts arbitrary temperature and velocity boundary conditions has been developed for this study and can be used to investigate two-dimensional convection in this parameter range. The model is written in terms of vorticity, stream function, and temperature, and the appropriate fluid equations are defined below. The vorticity and stream function are related to the velocity field by

$$\mathbf{q} = \hat{\jmath} \times \nabla \psi \quad \eta = \nabla \times \mathbf{q}$$

where  $\hat{\jmath}$  is the unit vector in  $+y$ ,  $\psi$  is the stream function, and  $\eta$  is vorticity. The dimensionless governing equations (5) through (7) become

$$\partial\eta/\partial t = J(\psi, \eta) - \sigma R_a \partial\theta/\partial x + \sigma \nabla^2 \eta \quad (30a)$$

$$\partial\theta/\partial t = J(\psi, \theta) + \nabla^2 \theta \quad (30b)$$

$$\nabla^2 \psi = \eta \quad (30c)$$

where  $J(\cdot)$  is the Jacobian operator  $\partial(\cdot)/\partial(x, z)$ .

The Prandtl number in the mantle is of the order of  $10^{24}$ , and thus equations (30) can be further simplified by representing the dependent variables by an asymptotic series in  $1/\sigma$ . The lowest-order problem becomes

$$\nabla^2 \eta_0 = R_a \partial\theta_0/\partial x \quad (31a)$$

$$\partial\theta_0/\partial t = J(\psi_0, \theta_0) + \nabla^2 \theta_0 \quad (31b)$$

$$\nabla^2 \psi_0 = \eta_0 \quad (31c)$$

The lowest-order solutions obtained from these equations are valid to order  $1/\sigma \approx 10^{-24}$ . The fact that this representation ignores the term  $\partial\eta/\partial t$  does not imply that  $\partial\eta/\partial t = 0$ , only that the term is not important in the primary balance of the vorticity equation. The vorticity is, in fact, a function of time, since its source term  $\partial\theta_0/\partial x$  is time dependent.

The numerical model is horizontally finite, and thus boundary conditions must be specified on two vertical planes. The complete nondimensional boundary conditions required to simulate Rayleigh-Benard convection are shown in Figure 5. The free boundary condition at  $z = 0, 1$  is replaced by  $\eta = 0$ , since the vorticity is proportional to  $\partial u/\partial z$  when  $w$  is constant on horizontal boundaries. The boundary conditions at  $x = 0$  and  $x = L$  results from considering an  $x$  domain extending from  $x = 0$  to  $x = 2L$  with periodic boundary conditions at both these points. Such boundaries simulate an annulus in which the effects of sphericity are ignored. The periodic boundary condition at  $x = 2L$  can be replaced by a symmetry condition on the temperature field and antisymmetry on the vorticity field at  $x = L$ . The details of the numerical formulation and method of solution of (31) are given in the appendix.

Figure 6 is an example of a steady, numerical solution to the Rayleigh-Benard problem at Rayleigh number 725. The result is presented in terms of the nondimensional temperature and stream-function field. The domain of calculation is horizontally finite, and thus only a discrete set of  $x$  wave numbers exists. The most unstable mode in this set has a critical Rayleigh number of 671.3;  $R_a = 725$  thus corresponds to  $\epsilon^2 = 0.08$ . A measure of the accuracy of the numerical method of solution can be obtained by comparing the amplitude

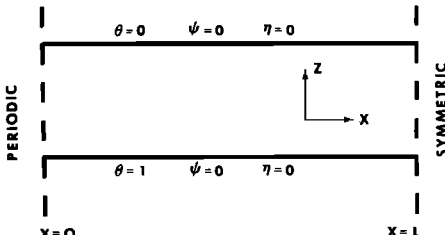


Fig. 5. Rayleigh-Benard convection model with boundary conditions in terms of stream function and vorticity.

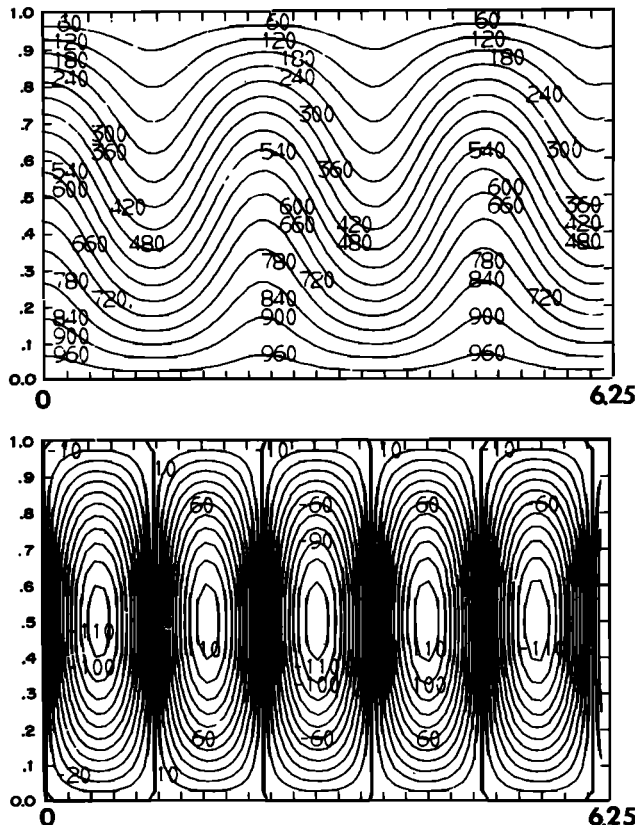


Fig. 6. Steady, free Rayleigh-Benard convection,  $R_a = 725$ .  
Top: temperature, contours from 0 to 0.96. Bottom: stream function, contours from 1.1 to -1.1.

predicted analytically by (27) and the numerical result. Equation 27 predicts a nondimensional amplitude of 3.07. The numerical amplitude is 3.00 and represents an error of only 2%. The accuracy with which the numerical method reproduces analytic results is even better at higher Rayleigh numbers. A test case with  $\epsilon^2 \approx 1$  indicates an accuracy greater than 1%. The agreement between analytic and numerical solutions results in a degree of confidence in the numerical model that standard numerical error estimates cannot provide.

The principal conclusions regarding Rayleigh-Benard convection can be summarized: (1) for  $\epsilon^2$  slightly greater than 0 and less than 12, periodic rolls are the preferred form of convection; (2) for  $\epsilon^2 > 12$ , a steady, two-dimensional model will not recover experimentally observed results; (3) the aspect ratio of the rolls is very nearly one [ $m_c = \pi/(2)^{1/2}$ ]; (4) the amplitude develops on a slow  $O(\epsilon^2)$  time scale.

The geologic consequences of these conclusions are now considered. The aspect ratio of the asthenosphere below a typical plate is of the order of 5 or greater, which suggests that the lithosphere is not the upper limb of a single

Rayleigh-Benard cell. Therefore, if the plates move as a result of Rayleigh-Benard convection, they must be driven by the integrated stress of many cells. The net force on a lithospheric plate can be written:

$$F(t) = \int_0^{L(t)} \sigma_x dx \quad (32)$$

where the center of spreading defines  $x = 0$  and  $\sigma_x$  is the stress at the base of the plate due to convection in the asthenosphere.  $L(t)$  is the horizontal dimension of the plate in the direction of spreading, which is a function of time. Figure 2 illustrates the dependence of horizontal dimensions on time. If the two ridges are fixed in space, the motion of each plate away from its respective ridge implies that the trench migrates to the left, and the plate on the right grows while the plate on the left shrinks.

Since the convective velocities are spatially periodic,  $\sigma_x$  will also be periodic, with wavelength smaller than typical plate dimensions, and thus there will exist dimensions  $L_n$  such that  $F(t) = 0$  when  $L(t) = L_n$ . Once  $F(t) = 0$ ,  $L(t)$  remains  $L_n$ , since the plate has no inertia when the Prandtl number is large. Spreading stops. Figure 7a shows the integrated stress resulting from convection versus plate length and indicates that stable lengths will occur whenever the plate dimension becomes a multiple of two cell widths.

The periodic nature of Rayleigh-Benard convection results in a second objection. The moving lithosphere implies a net mass transport from trench to ridge in the asthenosphere. A periodic flow with half-wavelength smaller than the trench to ridge length scale cannot satisfy such a mass transport criterion.

The most damaging property of Rayleigh-Benard convection in terms of its being a viable mechanism for driving sea floor spreading is the periodic nature of the flow and the order 1 aspect ratio of the cells. Can this objection be alleviated if a more realistic convection model were considered, one that would include internal heat sources and temperature-dependent fluid properties?

*Tritton and Zarraga [1967]*, in a qualitative experimental study of convection produced by uniform heating throughout the body of a fluid layer, observed that at large Rayleigh numbers the distance between rising and falling currents was as great as 5 times the depth of the layer. However, a preliminary theoretical study of the above experiment by *Roberts [1967]* and a subsequent numerical study by *Thirlby [1970]* fail to determine any dramatic increase in wavelength with increasing Rayleigh number. Also, experimental observations by *Hooper* [see *Thirlby, 1970*] do not show convective cell elongations on the scale of Tritton and Zarraga. The problem of internal heat sources has not yet been definitively resolved, but present understanding suggests that such heating will not remove the fundamental objections to convection in the present context.

Theoretical studies of convection with temperature-dependent fluid properties by *Palm [1960]* and *Busse [1967]* indicate that cells of hexagonal plan form may be preferred over two-dimensional rolls even for  $\epsilon$  order 1. The tendency toward hexagonal cells may not be effective in the presence of hori-

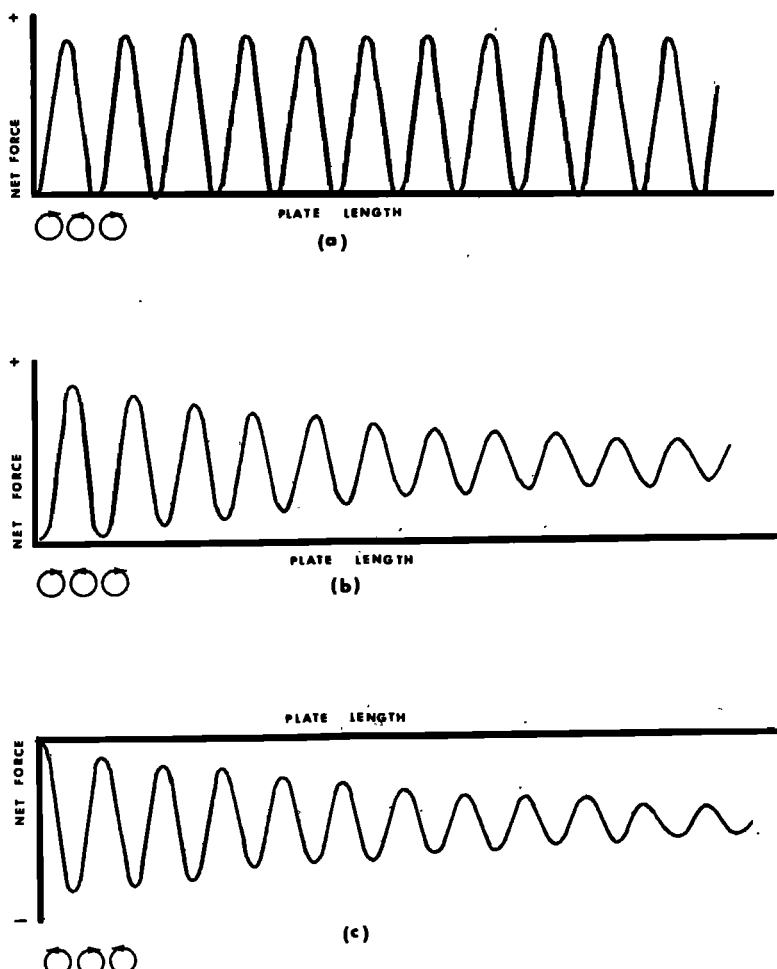


Fig. 7. Net force as a function of plate length. (+ indicates tension, — indicates compression). A few cells have been indicated to show phasing. (a) Rayleigh-Benard; convection; (b) modulated convection with optimum phasing; (c) modulated convection with worst possible phasing.

horizontal temperature gradients such as those existing at the edges of continents (section 4). The continental thermal gradients will tend to enhance rolls parallel to the continental margins. In any event, the aspect ratio of hexagonal cells will be order 1, and thus previous conclusions would still apply.

#### 4. ROLE OF HORIZONTAL TEMPERATURE GRADIENTS

It is generally accepted that continental crustal rocks are relatively rich in radiogenic heat sources compared with oceanic crustal rocks. Under these circumstances one expects that the heat flow at sea will be less than that observed in continental areas. It is therefore surprising to find that the heat

flow through the ocean floor is approximately equal to the mean heat flow through continents [Lee and Uyeda, 1965]. One possible explanation is that despite the near-surface enrichment of the continental crust, the mean composition and therefore the heat production is the same for both continents and oceans when a greater depth extent is considered [Bullard, 1952]. This possibility suggests that the excess heat sources in the continental crust are balanced by a depletion at depth.

The effect on the temperature field of concentrating heat sources near the surface can be explored by using a steady, one-dimensional heat flow equation with the constraint that both temperature and heat flow be uniform at the surface  $z = 0$  [Jeffreys, 1962]. Consider the equation

$$\kappa d^2 \theta / dz^2 + Q(z) = 0$$

where

- $\theta$  temperature
- $Q$  radiogenic heat source strength
- $\kappa$  thermal conductivity

The neglect of horizontal derivatives implies that the horizontal scales in the conduction problem are presumed large compared with the depth extent. With  $z$  increasing downward from  $z = 0$  at the surface, the above equation can be integrated, yielding

$$\kappa d\theta / dz = \int_z^\infty Q(\xi) d\xi + H_0$$

where  $H_0$  is independent of  $z$ . Since we require constant heat at the surface,

$$\int_0^\infty Q(\xi) d\xi + H_0 = \text{const}$$

The integral represents the total heat source strength in a column, and  $H_0$  represents the heat flow into the base of the column. This equation implies that if the heat flowing from the deep interior is constant for all columns ( $H_0 = \text{const}$ ), the uniformity of surface heat flow results from

$$\int_0^\infty Q(\xi) d\xi = Q_0$$

where  $Q_0$  is a constant for all columns.

A second integration results in the temperature solution

$$\theta_{(z)} = (1/\kappa) \int_0^z d\xi \int_\xi^\infty Q(\xi) d\xi + H_0 z / \kappa + \theta_0$$

where  $\theta_0$  is the surface temperature. Our main interest is the effect of the heat sources in the crust on the temperature in the asthenosphere, and thus we can consider the temperature at a depth  $z_0$ , below which no significant radiogenic heat sources exist.

$$\theta_{(z_0)} = (1/\kappa) \int_0^{\infty} d\xi \int_{\xi}^{\infty} Q(\xi) d\xi + H_0 z_0 / \kappa + \theta_0$$

Since no significant heat sources exist below  $z_0$ , the upper limit of integration can be replaced by infinity. If we reverse the order of integration and make use of the mean value theorem, the double integral can be written:

$$(1/\kappa) \int_0^{\infty} d\xi \int_{\xi}^{\infty} Q(\xi) d\xi = D_0 / \kappa \int_0^{\infty} Q(\xi) d\xi = D_0 Q_0 / \kappa$$

where  $D_0$  is a weighted mean depth of heat generation. The temperature solution can now be written in an easier to interpret form:

$$\theta_{(z_0)} = D_0 Q_0 / \kappa + H_0 z_0 / \kappa + \theta_0$$

We can thus explicitly see the effect of concentrating the heat sources near the surface while requiring uniform temperature and heat flow at the surface; it results in a lower temperature at depth. The geologic implication is that the distribution of heat sources in the crust results in relatively colder temperatures under continents than at similar depth under ocean basins. This is not a new conclusion: *MacDonald* [1963] considers the two-dimensional, time-dependent conduction problem and formally arrives at the same result. MacDonald's results show that horizontal temperature changes may be as large as 100°C at a depth of 100 km. The horizontal length scale over which the temperature varies is of the order of 1000 km. Despite the fact that MacDonald ignores the advection of heat in the asthenosphere, his results provide a useful estimate of horizontal temperature gradients at the base of the lithosphere (except near active ridges where the temperature depends on warm material intruded into the ridge axis). In a mathematical sense the temperature in the lithosphere is fully determined by the distribution of radiogenic heat sources and the surface temperature and heat flow boundary conditions, and thus it is independent of the ignored advection of heat in the asthenosphere. *Sclater and Francheteau* [1970] review recent observations of terrestrial heat flow and also suggest that they are indicative of higher temperatures in the upper mantle under ocean basins. For present purposes the two conclusions regarding the thermal state of the mantle that are important are that (1) horizontal temperature gradients exist in the upper mantle, and (2) these gradients are such that it is warmer under ocean basins than at similar depth under continents.

These conclusions suggest that the investigation of the role of horizontal temperature gradients as sources or modifiers of fluid motions in the asthenosphere is relevant. A question that can be considered at this time is, Can horizontal temperature gradients modify Rayleigh-Benard convection to the point that some of the objections raised in the previous section are removed? The first model problem of this section will show that horizontal temperature gradients can modulate the amplitude of Rayleigh-Benard convection and thus break the periodic nature of the flow.

a. *Modulated convection.* Consider the problem of an infinite layer of fluid between two free horizontal boundaries subject to a temperature boundary

condition that includes a weak spatial variation on a length scale that is long compared with the depth of the fluid. The model and boundary conditions are shown in Figure 8.

Since the spatial dependence of the boundary temperature is on a long  $x$  scale, order  $\beta$  compared with the depth of the fluid, a second length scale can be introduced as an independent variable  $X$ :

$$X = \beta x \quad (33)$$

Then derivatives with respect to the horizontal coordinate are written:

$$\partial/\partial x + \beta \partial/\partial X \quad (34)$$

The dimensionless, governing equations (5-7) become

$$\begin{aligned} u \partial u / \partial x + \beta u \partial u / \partial X + w \partial u / \partial z &= -\partial p / \partial x - \beta \partial p / \partial X + \sigma \nabla^2 u \\ &\quad + \sigma \beta^2 \partial^2 u / \partial X^2 + 2\sigma \beta \partial^2 u / \partial x \partial X \end{aligned} \quad (35a)$$

$$\begin{aligned} u \partial w / \partial x + \beta u \partial w / \partial X + w \partial w / \partial z &= -\partial p / \partial z + \sigma R_a \theta + \sigma \nabla^2 w \\ &\quad + \sigma \beta^2 \partial^2 w / \partial X^2 + 2\sigma \beta \partial^2 w / \partial x \partial X \end{aligned} \quad (35b)$$

$$w \partial \theta / \partial z + u \partial \theta / \partial x + \beta u \partial \theta / \partial X = \nabla^2 \theta + \beta^2 \partial^2 \theta / \partial X^2 + 2\beta \partial^2 \theta / \partial x \partial X \quad (35c)$$

$$\partial u / \partial x + \beta \partial u / \partial X + \partial w / \partial z = 0 \quad (35d)$$

As in Rayleigh-Benard convection, we must restrict the analysis to small amplitudes. We define

$$\epsilon = (R_a - R_c)^{1/2}/R_c$$

The dependent variables are expanded as before in an asymptotic series in  $\epsilon$ , and this representation is substituted into the governing equations (35). In order to extract the appropriate equation for each order in  $\epsilon$ , a specific choice of  $\alpha$  and  $\beta$  in terms of  $\epsilon$  is required. We choose

$$\alpha = \epsilon^2 \quad \beta = \epsilon \quad (36)$$

This choice is motivated by the fact that it results in a problem in which the temperature variations on the boundary affect the order  $\epsilon^2$  velocity field. This is clearly not a unique choice, but the solution resulting from this choice will also show the effect of considering  $\alpha < \epsilon^2$  and  $\beta < \epsilon$ .

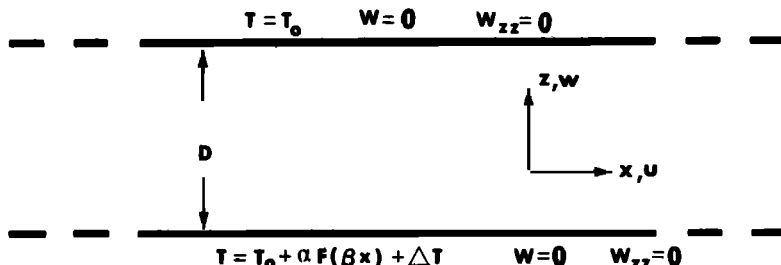


Fig. 8. Modulated convection model.

The modulated convection problem parallels the Rayleigh-Benard problem up to order  $\epsilon^2$ , for it is not until this order that the new boundary condition and length scale enter the problem. The lowest-order solution is again the purely conductive state with no fluid motion. The order  $\epsilon$  solutions are modified only in that the amplitude coefficients  $A$  and  $B$  now become functions of the long space scale. Thus

$$w_1 = (A_{(x)} \cos mx + B_{(x)} \sin mx) \sin \pi z \quad (37)$$

Other problems in which convective amplitudes depend on long space scales have been studied by *Segel [1969]* and *Newell and Whitehead [1969]*.

If the  $\epsilon^2$  problem is stated in terms of  $w_2$  alone, as before, the nonlinear terms can be evaluated and are found to cancel:

$$\mathcal{L}(w_2) = 0 \quad \mathcal{L}(\ ) = \sigma \nabla^6 - \sigma R_c \partial^2 / \partial x^2 \quad (38)$$

As a normalization condition we choose  $w_2 = 0$ . The temperature has to satisfy an inhomogeneous boundary condition at this order ( $\theta_2 = F_{(x)}$ ,  $z = 0$ ), and we find

$$\begin{aligned} \theta_2 = & - \frac{[A_{(x)}^2 + B_{(x)}^2]}{8\pi(m^2 + \pi^2)} \sin 2\pi z - \frac{2m}{(m^2 + \pi^2)} (dA/dX \sin mx - dB/dX \cos mx) \\ & \cdot \sin \pi z + (1 - z)F_{(x)} \end{aligned} \quad (39a)$$

$$u_2 = -\pi/m^2(dA/dX \cos mx + dB/dX \sin mx) \cos \pi z \quad (39b)$$

The order  $\epsilon^3$  problem stated in terms of  $w_3$  alone is not homogeneous, since the nonlinear terms do not cancel. The equation for  $w_3$  has the general form

$$\begin{aligned} \mathcal{L}(w_3) = & \Delta_{(x)} \cos mx \sin \pi z + \Gamma_{(x)} \sin mx \sin \pi z \\ & + \text{terms in } \sin n\pi z, \cos nm x, \sin nm x \end{aligned} \quad (40)$$

where  $n \geq 2$ . As before, the necessary condition that  $\Delta_{(x)} = 0$  and  $\Gamma_{(x)} = 0$  leads to amplitude equations for  $A_{(x)}$  and  $B_{(x)}$ . These equations can be written in terms of  $R_{(x)}$  and  $\phi_{(x)}$ , where

$$R_{(x)} \exp[i\phi_{(x)}] = A_{(x)} + iB_{(x)} \quad (41)$$

The amplitude equations are

$$d\phi/dX = K/R_{(x)}^2 \quad (42a)$$

where  $K$  is an undefined constant, and

$$\begin{aligned} 6\pi^2 d^2R/dX^2 - 6\pi^2 R_{(x)} (d\phi/dX)^2 + (m^2 + \pi^2)^2 R_{(x)} [1 + F_{(x)}] \\ - (1/8)(m^2 + \pi^2)R_{(x)}^3 = 0 \end{aligned} \quad (42b)$$

Equation 42 reduces to the amplitude equation for 'pure' Rayleigh-Benard convection (23) when  $F_{(x)} = 0$  and  $A$  and  $B$  are constants.

The amplitude equations can be reduced to a simpler form if we restrict  $F_{(x)}$  to be localized. Since the fluid is horizontally infinite, we expect that, far from the region where the boundary temperature varies, the Rayleigh-Benard solution with constant amplitude and wave number  $m_c$  should be recovered.

This implies that  $K$  in (42a) can be set to 0. The amplitude is now determined by the single equation

$$6\pi^2 d^2R/dX^2 + (m^2 + \pi^2)^2[1 + F_{(X)}]R_{(X)} - (1/8)(m^2 + \pi^2)R_{(X)}^3 = 0 \quad (43)$$

The phase  $\phi$  is an undetermined constant, which implies that  $F_{(X)}$  is sufficiently smooth on the length scale of the cells so as not to determine the phase of the solution.

For sufficient separation between the scale of  $x$  and  $X$ , one would expect the convective amplitude to depend on the 'local' Rayleigh number  $R_a[1 + F_{(X)}]$ . The neglect of the differentiated term in the amplitude equations (42) results in such a local Rayleigh number approximation. Had we considered the case  $\beta < \epsilon$  in our original formulation, the differentiated term would not enter the amplitude equation at all. This suggests as a rule of thumb for evaluating the effect of 'weak' horizontal gradients on Rayleigh-Benard convection the use of a local Rayleigh number approximation.

Equation 43 can be easily solved numerically by using a relaxation technique that requires the amplitude far from the boundary temperature variation to be that of simple Rayleigh-Benard convection. An example of such a solution is shown in Figure 9 for  $F_{(X)} = \operatorname{sech} X$ . The local Rayleigh number solution is also shown and confirms its usefulness as a measure of modulated amplitude.

The validity of both the asymptotic theory and the restricted set of solutions considered in the previous discussion can be tested by solving the same model problem by means of numerical techniques. The numerical model developed for this study (see the appendix) accepts arbitrary boundary conditions and thus can be used to investigate the model shown in Figure 8. The domain

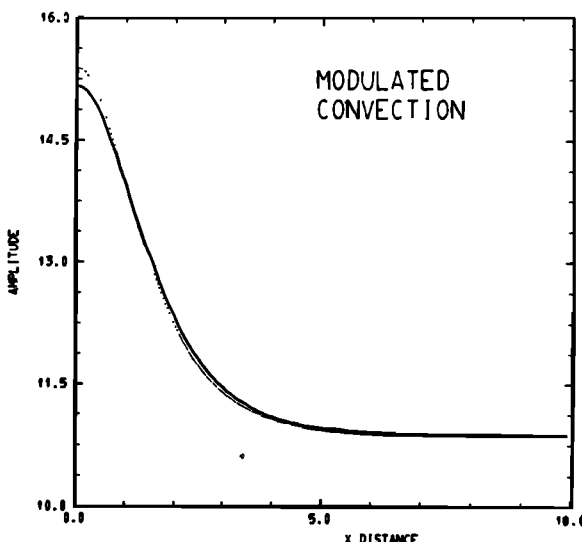


Fig. 9. Modulated amplitude  $R_{(X)}$  as a function of  $X$  when  $F(X) = \operatorname{sech} X$ . Local Rayleigh number approximation shown as dotted curve.

of calculation can no longer be horizontally infinite, and therefore periodic boundary conditions are imposed on two vertical planes in the fluid. Figure 10 shows the resulting steady, nondimensional temperature, temperature boundary condition, and stream function field over the left half of the complete domain for  $R_a = 725$ . If the temperature boundary condition is considered symmetric

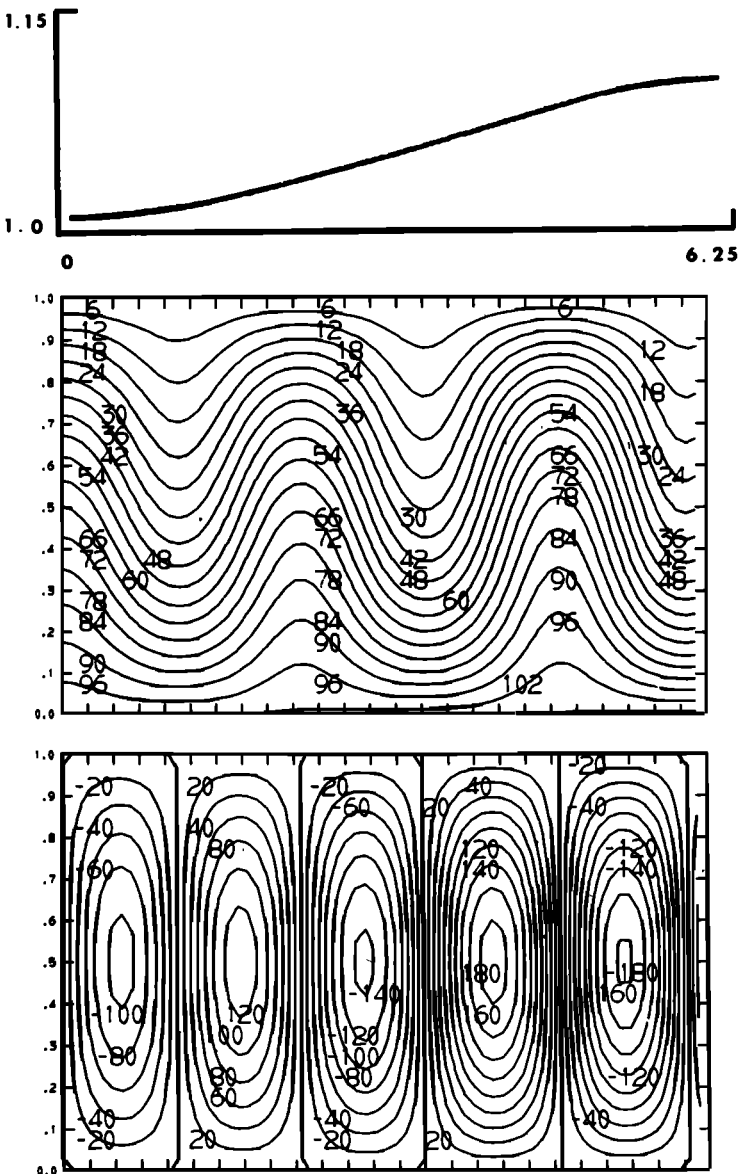


Fig. 10. Steady numerical solution to modulated convection problem,  $R_a = 725$ . Top: temperature boundary condition at  $z = 0$ . Middle: temperature, contours from 0 to 1.15. Bottom: stream function, contours from  $-1.8$  to  $1.8$ .

about  $x = 6.25$ , then the temperature field is symmetric and the stream function is antisymmetric about this point. The amplitude of the cells, as shown by the streamlines, is modulated on the length scale of the boundary temperature variations. Despite the limitation imposed by the small separation of scales between the boundary temperature variation and the depth of the fluid, numerical and analytical results never differ by more than 4% for any  $X$ . The small separation of the two length scales does induce a slight dependence of the wave number on  $X$  that is not predicted by the analytical solution (which assumed a large separation between the two length scales). The agreement between the analytical and numerical solutions is sufficiently good to argue that modulated convection is the physically realizable result of weak, long-scale temperature variations on the boundaries of a convecting fluid.

Modulated convection has the desirable property that the cells and thus the resulting stresses (if no-slip boundaries had been considered) are no longer periodic. The objection to Rayleigh-Benard convection based on the existence of stable plate dimensions can therefore be removed by including horizontal temperature variations on the boundaries of the fluid layer. Figure 7b, c shows how the modulated amplitude can result in net forces for all plate dimensions. If the cells are phased in such a manner that upwelling is maintained under the ridge axis, net tensional forces are applied to the plates on either side of the ridge. On the other hand, the requirement of a net mass transport from trench to ridge in the asthenosphere is not satisfied by this model. The modulated convection problem need not be discarded on this basis, for if its role is restricted to generating stresses that initiate continental breakup, no mass flux requirement arises. By 'breakup' I mean the original splitting of a large continent such as South America-Africa as the first stage of sea floor spreading. I shall return to this application of the modulated solution.

There is no a priori reason why the role of horizontal gradients should be restricted to modifying flows that result from other sources. It is well known that horizontal temperature gradients, however weak, result in fluid motions; this is in contrast to vertical temperature gradients, which must exceed a critical value. The next series of model problems investigates the motion of a fluid layer driven primarily by horizontal temperature gradients on the boundaries.

*b. Horizontal convection.* The role of horizontal temperature gradients as the principal source of motion can be investigated by using the same numerical model used in the study of modulated convection. The only modification required is that the Rayleigh number based on the vertical temperature difference be less than critical. The horizontal temperature gradients in the body of the fluid are generated by considering nonuniform temperatures on the upper boundary.

Figure 11 is an example of horizontal convection (convection driven primarily by imposed horizontal temperature gradients). The nondimensional temperature at  $z = 0$  is one; the temperature at  $z = 1$  varies as a function of  $x$  as shown in Figure 11. The solution displayed is the steady, nondimensional temperature and stream function field for free boundaries and for Rayleigh

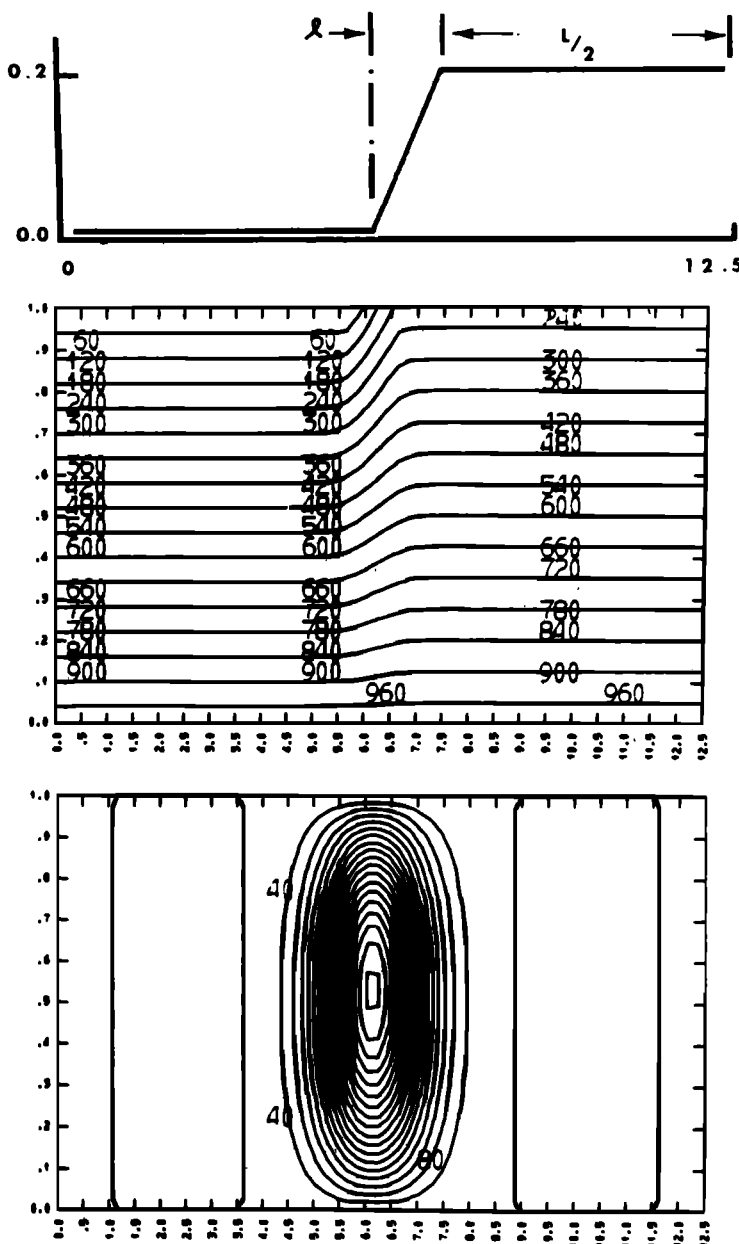


Fig. 11. Steady horizontal convection with  $R_a = 100$ ,  $L \approx 11D$ ,  $l \approx D$ . Top: temperature boundary condition at  $z = 1$ . Middle: temperature, contours from 0 to 0.96. Bottom: stream function, contours from 0 to 0.072.

number equal to 100. As in previous numerical calculations, the temperature field is symmetric and the stream function is antisymmetric about  $x = 12.5$ ;  $x = 0$  is a periodic boundary.

The circulation resulting from the horizontal temperature variation on the boundary is counterclockwise, and thus the flow at small depth is from hot to cold. This well-known result becomes very important if we recall that earlier arguments suggested that the temperature under continents is relatively cold. The horizontal temperature gradients in the asthenosphere due to the concentration of radiogenic material in the continental crust force a flow that, at the base of the lithosphere, is from ocean to continent. Such a flow would inhibit the breakup of preexisting continental masses such as South America–Africa by resulting in net compressive forces. We shall return to this point after other properties of horizontal convection are established.

A second property of horizontal convection is the aspect ratio of the resulting cell. In the example shown in Figure 11, the aspect ratio is about three. There are three imposed length scales in the problem that conceivably can determine the width of the cell. The depth  $D$  is one, and the other two ( $L$  and  $l$ ) are specified by the temperature on the upper boundary. In Figure 11,  $l \approx D$  and  $L \approx 11D$ . A series of numerical experiments were carried out in an effort to determine which of the three length scales controls the width of the cell. It was found that in the range  $L > 2D$ ,  $l \leq D$ , the depth is the determining factor. Figure 12 is an example of a steady case where  $l \approx D/2$ ,  $L \approx 5$ . The temperature is zero at  $z = 0$  and varies as a function of  $x$  as shown at  $z = 1$ . The cell shown in Figure 12 has virtually the same structure as that in Figure 11 despite different imposed horizontal length scales and basic stratification. Figures 11 and 12 can therefore be regarded as typical of the structure one would expect when  $L > 2D$  and  $l \leq D$ . These restrictions on the horizontal scales of the temperature field are satisfied in the asthenosphere if a depth extent of the order of 1000 km is considered.

The principal properties of horizontal convection that are important to the problem of motions in the asthenosphere are (1) the sense of a horizontal convection cell is such that at shallow depth the flow is from hot to cold; and (2) the width of the cell is approximately 3 times the depth of the fluid layer.

Having gained an understanding of the role of horizontal temperature gradients as primary sources of motion or as modifiers of flows driven by other sources, we can ask what role they play in the asthenosphere. It is premature to consider the horizontal temperature gradients in connection with present-day sea floor spreading dynamics, since the problem of net mass transport in the asthenosphere has not yet been resolved. For the moment we can only consider the role of these gradients in effecting the original breakup of large continental masses.

*c. Breakup problem.* Many authors (most recently *Ichiye* [1971]) have commented on the possibility that the horizontal temperature gradients at the edges of continents drive flows in the asthenosphere which ‘break’ the original continents by generating net tensional forces. This suggestion is not consistent

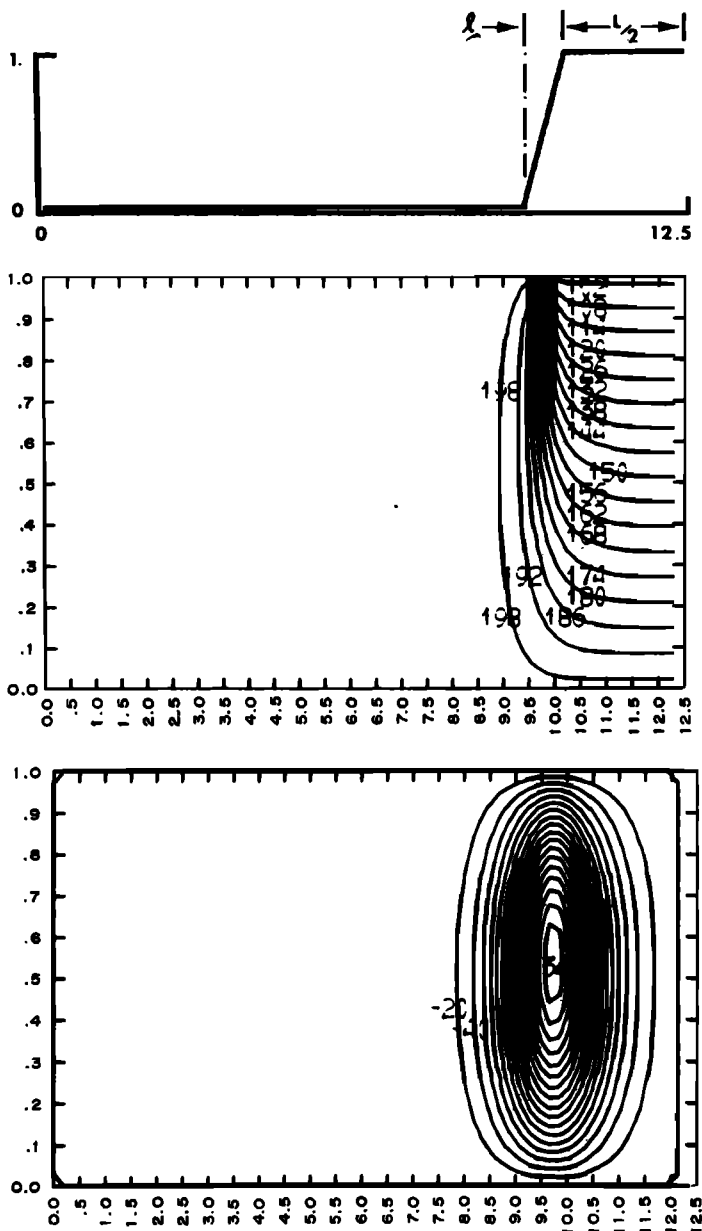


Fig. 12. Steady horizontal convection with  $R_a = 100$ ,  $L \approx 5D$ ,  $l \approx D/2$ . Top: temperature boundary condition at  $z = 1$ . Middle: temperature, contours from 1.02 to 1.98. Bottom: stream function, contours from 0 to  $-0.34$ .

with the understanding of horizontal convection derived from the previous section. It has been shown that if the thermal structure of the earth is such that the temperature under continents is relatively cold compared with the temperature at similar depths under ocean basins, then the thermally driven edge cells subject the continental lithosphere to net compressive forces. A similar conclusion regarding the stabilizing effect of edge cells at continental margins results from a linear analysis (ignoring heat advection) by Allan *et al.* [1967]. Rather than use horizontal temperature gradients to explain the original breakup of large continents, we are faced with the problem of suggesting a mechanism capable of overcoming the stabilizing effect of these gradients.

The modulated convection problem suggests a possible mechanism. If at some deep level in the mantle the temperature is horizontally uniform, the relative coolness under continents results in a locally higher Rayleigh number. If the original continental mass is sufficiently large, the edge cells, which have an aspect ratio of 3, will not occupy the entire region under the continent. There will be room for counterrotating (tension producing) Rayleigh-Benard cells. The hope is that a parameter range exists in which the inner Rayleigh-Benard cells can overcome the adverse effect of the edge cells. The modulated convection problem does not define the desired parameter range because it required horizontal temperature variations on a scale that is large compared with the depth, which probably is not the case for the asthenosphere.

There are too many variables to allow for a systematic mapping of the complete parameter fields. Thus a limited number of cases were considered, and the parameter range was chosen primarily by experience. The solutions are obtained using the same numerical model used to investigate modulated convection. The one modification required is a change in the dynamic boundary condition at  $z = 1$  from 'free' ( $\partial u / \partial z = 0$ ) to 'rigid' ( $u = 0$ ). The stress, or equivalently the vorticity, will no longer be 0 at  $z = 1$ , and therefore the net force on an overlying plate can be estimated. The presence of a continent is modeled by its effect on the temperature boundary condition on the upper surface of the fluid layer.

Figure 13 shows the result for a calculation that considers a continental temperature anomaly 4 times the depth scale wide and 20% of the total vertical temperature change in amplitude. The stream function field shown is still in the process of spinning up. The time evolution to this time step is (1) horizontal convection cell at  $x = 10.5$  spins up first; (2) the Rayleigh-Benard cell under the continent follows, since it is in a region of relatively high Rayleigh number; and (3) finally, Rayleigh-Benard cells appear in the low Rayleigh number region as momentum diffuses away from the horizontal convection cell.

The stress (measured by the vorticity) on an overlying plate at  $z = 1$  can be integrated away from the center of the continental temperature anomaly and thus provides an estimate of the total force as a function of plate length. As shown in Figure 13, the flow results in a net tensional force on the plane of symmetry of the continent if lengths greater than 5 times the depth are considered. The total dimensional force is of the order of  $10^{13}$  dynes (using  $\nu = 10^{21}$ ,  $\kappa = 10^{-2}$ , and  $D = 10^8$  cgs).

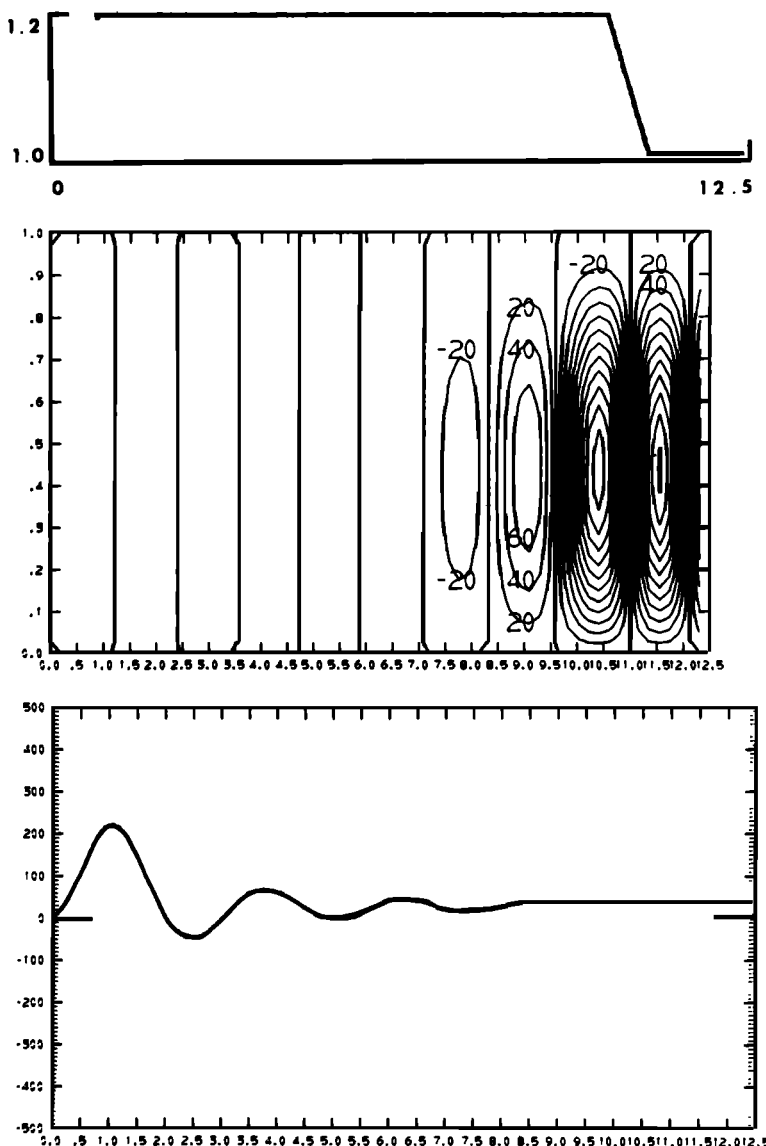


Fig. 13. Breakup model for continent 5D wide centered at  $x = 12.5$  and maximum vertical Rayleigh number of 1500. Top: temperature boundary condition at  $z = 1$ . Middle: stream function, contours from -2.2 to 2.2. Bottom: integrated stress as a function of distance from plane of symmetry of continent ( $x = 12.5$ ).

This type of model for the initiation of sea floor spreading has both attractive and troublesome aspects. In its favor is the fact that it predicts that only large continental masses, capable of accommodating the inner, counterrotating Rayleigh-Benard cells, are potentially unstable. Smaller continents (fragments of the original breakup) would be very stable, since the horizontal convection

cells at their edges would extend under the entire continent and thus insure stability. It would be interesting to investigate if the still large Europe-Asia complex shows evidence of further breakup. A troublesome aspect is that such a model may require a long time to develop, since the existence of tensional forces will depend on the Rayleigh-Benard 'spin-up' time.

The overall conclusion is that, given an appropriate parameter range, the stabilizing effect of edge cells can be overcome if a sufficiently large continent is considered.

The model problems considered in this section, which suggest a possible mechanism for effecting the original breakup of continents, are no longer valid once the lithosphere begins to move away from the center of spreading. The moving lithosphere requires a new dynamic boundary condition ( $u \neq 0$ ) at the top of the asthenosphere and a mass flux into (at trenches) and out of (at the ridge axis) the asthenosphere. The final section of this study will consider models that include these conditions, but before proceeding to these I shall first consider the dynamic role of mineralogical phase changes in the upper mantle. Phase changes act as sources and sinks of both buoyancy and heat, and it is important to understand if their effect on fluid motions is sufficiently large that it must be included in the formulation of the final model problems.

##### 5. ROLE OF PHASE CHANGES IN THE ASTHENOSPHERE

Seismic results indicate a series of transitions or 'discontinuities' in the mantle that can be interpreted in terms of phase changes in olivine, pyroxene, and garnet [Anderson, 1970]. The dynamic role of such phase changes as modifiers of fluid motions has been the subject of heuristic arguments for many years [Knopoff, 1964; Verhoogen, 1965; Ringwood, 1972]. The effect of a phase change on the stability of a layer of fluid heated from below was first studied analytically by Busse and Schubert [1971], who used a linearized model. Schubert and Turcotte [1971] subsequently applied the analysis to the olivine-spinel transition in the upper mantle.

The principal result of the linear analysis by Schubert and Turcotte is summarized by a stability diagram for Rayleigh-Benard convection through a phase boundary (Figure 14). The parameters are defined:

$Ra$  Rayleigh number;  $Ra = (g\alpha \Delta TD^3/\kappa\nu)$ .

$S$  a measure of the density difference between the two phases;

$$S = \Delta\rho/[(\alpha D/2)(\rho g/\gamma - \beta)].$$

$R_q$  Rayleigh number based on energy released by material changing phase;

$$R_q = g\alpha(Q/\rho C_p)D^3/\kappa\nu.$$

where  $g$ ,  $\alpha$ ,  $\kappa$ ,  $\nu$ ,  $\Delta T$ ,  $\rho$ , and  $D$  have the meanings given previously, and

$\Delta\rho$  density difference between the two phases.

$Q$  heat production (or loss) per unit mass of material changing phase.

$\beta$  vertical temperature gradient.

$\gamma$  slope of Clapeyron curve;  $\gamma = dP/dT = Q_{\rho_1\rho_2}/T \Delta\rho$ .

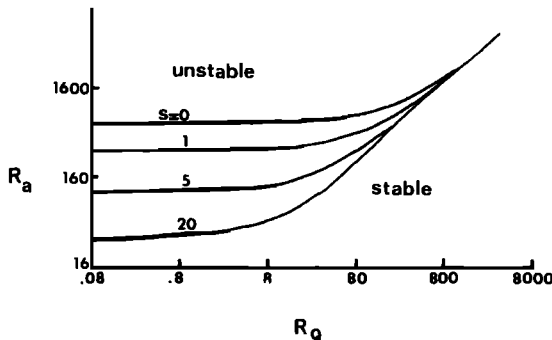


Fig. 14. Stability fields for convection through a phase boundary [after Schubert and Turcotte, 1971].

The effect of a given phase change on the stability of the system can be estimated by comparing the appropriate point on the family of neutral curves to the point  $S = 0$ ,  $R_q = 0$ , which is the critical Rayleigh number ( $R_c$ ) for the equivalent single-phase system. The family of neutral curves indicate that whenever  $R_q < 80$  the effect of the phase change is destabilizing. For  $R_q > 80$ , the two-phase system is more stable than a one-phase system, but convection through the phase boundary is certainly still possible. The phase boundary will appear to be a barrier to vertical motions only if the critical Rayleigh number for the two-phase system is greater than the Rayleigh number required for either phase to convect alone. Since the depth extent of each phase is less than the depth of the system as a whole, the Rayleigh number required for either phase to convect separately is always greater than  $R_{\beta\text{crit}}$ . The extreme case occurs when the phase boundary is at the midpoint of the layer, in which event the Rayleigh number required for separate convection is  $16R_{\beta\text{crit}}$ .

The analytical linear theory is capable of resolving the neutral curve for convection through a phase boundary but cannot determine the amplitude of finite solutions. We wish to determine both the dynamic role of a phase change and the effect of a velocity field on the local elevation of the phase boundary, and therefore a finite-amplitude, nonlinear theory is required.

Rather than formulate a two-layer model, with each layer representing a phase, we shall consider that the phase change occurs over a finite transition region. This representation results in a continuous density function that is much easier to treat mathematically. The model considered is shown in Figure 15.

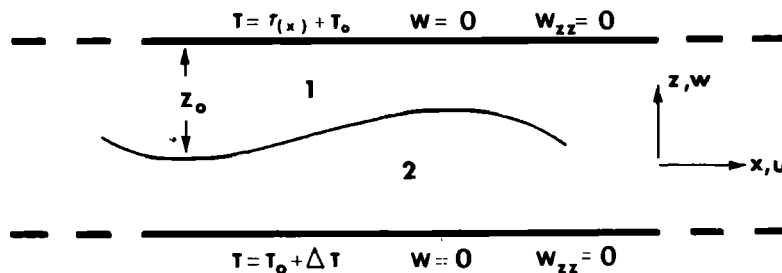


Fig. 15. Model for convection through a phase boundary.

If  $\theta$  is defined as

$$\theta = (T - T_0)/\Delta T \quad (44)$$

then

$$\rho = \rho_1[1 - \alpha\Delta T\theta + \Delta\rho\Gamma(x, z)] \quad (45)$$

where

$$\Delta\rho = (\rho_2 - \rho_1)/\rho_1 \quad (46)$$

and  $\Gamma(x, z)$  is the fractional concentration of phase 2. If  $\Delta\rho \ll 1$  and  $\alpha \ll 1$ , then the momentum equation after the Boussinesq approximation becomes

$$D\mathbf{q}/Dt = -PD^2/\rho_1\kappa^2\nabla\rho' + \frac{g\alpha}{\kappa^2}\frac{\Delta TD^3}{\kappa^2}\theta\hat{k} - \frac{\Delta p g D^3}{\kappa^2}\Gamma(x, z)\hat{k} + \nu/\kappa\nabla^2\mathbf{q} \quad (47)$$

which can be transformed into a vorticity equation, yielding

$$\nabla^2\eta = J(\psi, \eta) - \sigma R_a \partial\theta/\partial x + \sigma R_p \partial\Gamma/\partial x + \sigma\nabla^2\eta \quad (48)$$

where  $R_p = g\Delta\rho D^3/\kappa\nu$  and  $\sigma = \nu/\kappa$ . Because of the large Prandtl number, equation 48 can be approximated by

$$\nabla^2\eta = R_a \partial\theta/\partial x - R_p \partial\Gamma/\partial x + O(1/\sigma) \quad (49)$$

The temperature equation must be modified to take into account the energy absorbed or released as material changes phase. This heat production can be written:

$$Q_L = \rho q_L DT/Dt \quad (50)$$

where  $\Gamma$  is a measure of the concentration of phase 2, and  $q_L$  is the heat released per unit mass of material changing from phase 1 to phase 2.

The nondimensional temperature equation becomes

$$\partial\theta/\partial t = J(\psi, \theta - R_0/R_a\Gamma) + R_q/R_a \partial\Gamma/\partial t + \nabla^2\theta \quad (51)$$

where

$$R_q = \frac{g\alpha(q_L/C_p)D^3}{\kappa\nu}$$

The stream function and vorticity are related by

$$\nabla^2\psi = \eta \quad (52)$$

Equations 48, 51, and 52 are no longer sufficient, since a new dependent variable  $\Gamma$  is now in the problem. Another relationship is required, and it is provided by the Clapeyron curve, which specifies the phase boundary in temperature and pressure coordinates. If we know the temperature field  $T(x, z)$ , we can find a function  $Z_0(x)$  such that  $T[x, Z_{0(z)}]$  is always on the Clapeyron curve. The function  $Z_{0(z)}$  can be interpreted as the depth to the phase boundary. If we define the phase boundary as the  $\Gamma = 0.5$  (50% concentration of each phase) surface, then  $Z_{0(z)}$  determines the  $x$  dependence of  $\Gamma(x, z)$ . The vertical structure of  $\Gamma(x, z)$  is arbitrary

and is chosen so as to provide a transition zone of reasonable thickness. This uncertainty in the vertical structure of  $\Gamma(x, z)$  is not very important in the problem we are considering. We can see from (49) that  $\partial\Gamma/\partial x$  is a source term in a Poisson equation, and therefore, as long as the phase transition zone thickness is small compared to the total depth of the fluid, the exact vertical structure of  $\Gamma$  is unimportant compared to the total change in  $\Gamma$  across the zone. The same argument regarding total source strength versus exact source distribution can be made in connection with the temperature equation (51).

The equations governing a two-phase system are 49, 51, 52, and the Clapeyron relation. This set of equations, along with the boundary conditions shown in Figure 15, have been solved numerically for two classes of problems: (1) horizontal convection driven primarily by temperature variations on the boundaries, and (2) Rayleigh-Benard convection. Horizontal convection is the more useful of the two in estimating the effect of the phase change on the structure of the resulting flow. Horizontal convection has more freedom in its horizontal structure than Rayleigh-Benard convection which is limited to a discrete wave-number spectrum by the finite horizontal dimension of the domain of calculation. The Rayleigh-Benard model on the other hand has the important advantage that it will provide an estimate of numerical accuracy when compared with analytical results.

Figure 16 is typical of horizontal convection through a phase boundary. The nondimensional temperature and stream function fields are shown, as well as the dimensional change in elevation of the  $\Gamma = 0.5$  surface (when the depth is dimensionalized using  $D = 1000$  km). The temperature boundary conditions are  $\theta = 1$  at  $z = 0$  and  $\theta$  ranging from 0 to 0.2 at  $z = 1$ , as indicated by the intersection of the isotherms with the boundary. The dynamic boundary conditions are  $w = 0$  and  $w_{zz} = 0$  (free) at  $z = 0$  and  $z = 1$ . Periodic boundary conditions are imposed at  $x = 0$  and  $x = 25$ , which are satisfied by considering the temperature to be symmetric and the stream function antisymmetric around  $x = 12.5$ . The concentration function  $\Gamma(x, z)$  is such that the transition from one phase to another occurs over a depth of  $0.1D$ . The constant  $T_0$  must also be specified because together with  $\Delta T$  it determines the mean depth of the phase boundary. In the case shown in Figure 16,  $T_0$  is  $1200^\circ\text{C}$ , and the remaining parameters,  $R_a$ ,  $R_p$ , and  $R_q$ , have values of 100, 1600, and 24, respectively. The slope of the Clapeyron curve ( $Q_L \rho_1 \rho_2 / \Delta \rho T$ ) is determined once  $R_q$  and  $R_p$  are specified. A slope of  $6^\circ\text{C km}^{-1}$  is consistent with the above values of  $R_q$  and  $R_p$ . This slope, which we shall consider constant, is approximately the estimated value for the forsterite-spinel transition [Anderson, 1970].

To get an idea of the effect of the phase change in this parameter range, we can compare Figure 16 with Figure 11, which is the same calculation with  $R_p$  and  $R_q$  set to 0. The phase change increases the amplitude by a factor of 3, but the structure of the solution is unchanged. The increased amplitude when the phase change is present is not surprising. The family of neutral curves in Figure 14 suggest that the case  $R_q = 24$ ,  $R_p = 1600$  ( $S = 2$ ) is more unstable than  $R_q = 0$ ,  $R_p = 0$ . The depth to the phase boundary as measured by the  $\Gamma = 0.5$  surface is greater in warmer regions of the fluid, which one would expect for all cases with positive Clapeyron slope.

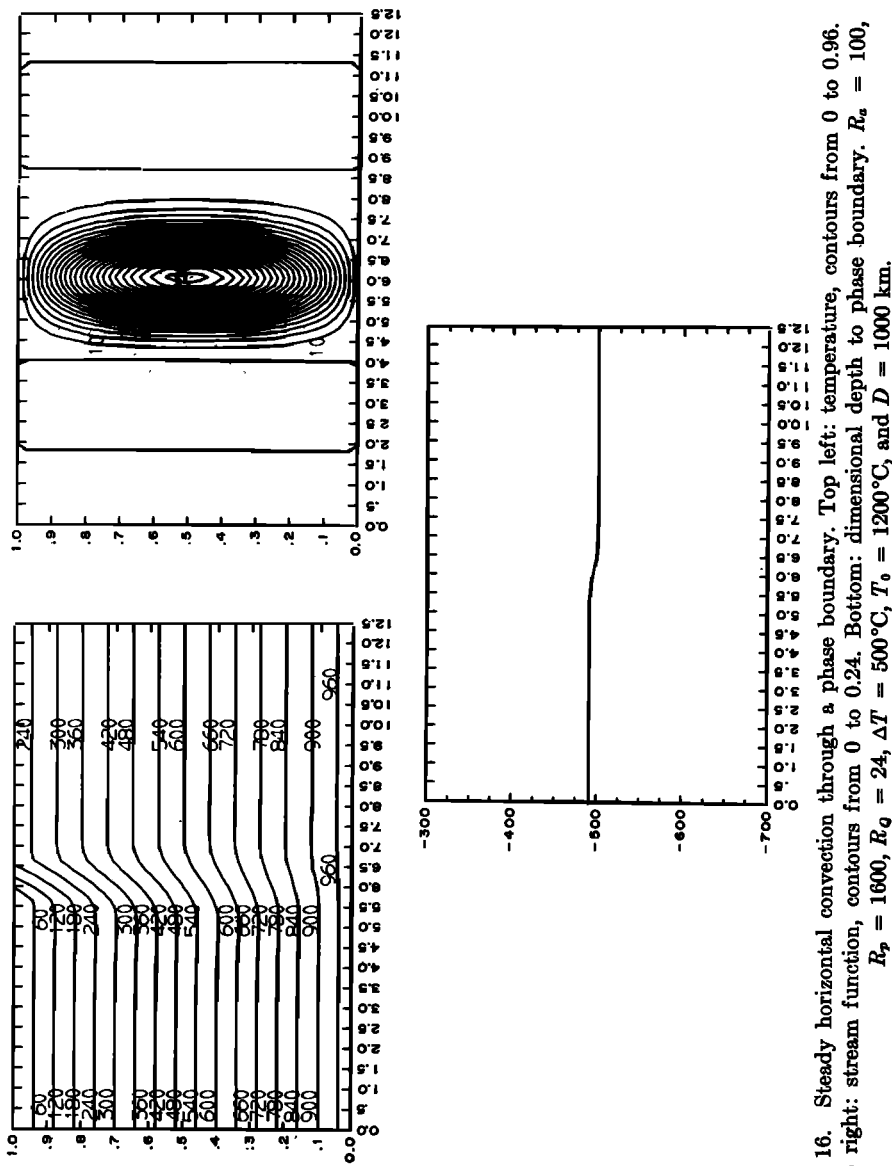


Fig. 16. Steady horizontal convection through a phase boundary. Top left: stream function, contours from 0 to 0.24. Top right: temperature, contours from 0 to 0.96. Bottom left: stream function, contours from 0 to 0.24. Bottom right: dimensional depth to phase boundary.  $R_s = 100$ ,  $R_p = 1800$ ,  $R_Q = 24$ ,  $\Delta T = 500^\circ\text{C}$ ,  $T_0 = 1200^\circ\text{C}$ , and  $D = 1000$  km.

Figure 17 shows the effect of varying the Rayleigh number on the amplitude of horizontal convection. The amplitude can be seen to be a linear function of  $R_a$ , as one would expect in a forced problem. For comparison, the amplitude versus  $R_a$  curve for  $R_q = 0, R_p = 0$  is also shown. One can see that the effect of the phase change is to increase the amplitude by a factor of about 3. In all the cases considered in making the graphs in Figure 17, no effect of the phase change on the structure of the resulting flow was observed. The overall conclusion is that a phase change in the parameter range considered increases the amplitude by a factor of 3 but does not change the structure of the flow.

We now proceed to consider the effect of a phase change on Rayleigh-Benard convection. Two groups of numerical experiments were considered. The first group was designed to determine the critical Rayleigh number of Rayleigh-Benard convection through a phase boundary. The numerically determined critical Rayleigh number can then be compared with the appropriate point on the family of neutral curves in Figure 14. The second group of experiments explore the finite amplitude regime.

The critical Rayleigh number for the two-phase system was estimated by varying the Rayleigh number until two values sufficiently close together were found such that perturbations grew for one value and decayed for the other. The growth or decay of the perturbations was determined by observing the temperature and vorticity field over long periods of time. Such a method of estimating the critical Rayleigh number is very costly in terms of computer time owing to the small growth or decay rates near the neutral curve. For this reason, only three cases were considered:

$$R_q = 0 \quad S = 2$$

$$R_q = 240 \quad S = 0$$

$$R_q = 100 \quad S = 2$$

In all three cases the phase change occurs at a mean depth of  $D/2$  (specified

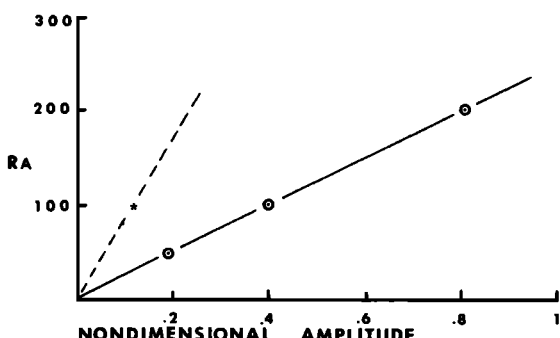


Fig. 17. Amplitude of horizontal convection through a phase boundary as a function of the Rayleigh number. Asterisk indicates  $R_q = 0$  and  $R_p = 0$ . Dotted circle indicates  $R_q/R_s = 0.24$  and  $R_p/R_q = 6.67$ .

by  $T_0$ ) and the boundaries are free so that the numerical model reproduces the same problem considered in the linear theory.

The numerical critical Rayleigh numbers can be compared with their analytically predicted value by plotting them on a graph of the relevant analytical neutral curves as shown in Figure 18. The excellent agreement between the numerical results and the linear theory can be taken as a measure of the accuracy of the numerical techniques used. As was previously discussed, the choice of a finite phase transition zone of thickness  $0.1D$ , instead of a sharp discontinuity as assumed in the linear theory, has no observable effect on the stability of the fluid.

We now consider the finite-amplitude regime. Figure 19 shows a typical case of steady Rayleigh-Benard convection through a phase boundary. The boundary conditions are

$$\theta = 0 \quad w = w_{zz} = 0 \quad z = 1$$

$$\theta = 1 \quad w = w_{zz} = 0 \quad z = 0$$

Periodic boundary conditions are imposed at  $x = 0$  and  $x = 25$ , which are satisfied if the temperature field is symmetric and the stream function is anti-symmetric about  $x = 12.5$ . The nondimensional parameters are  $R_a = 500$ ,  $R_p = 800$ , and  $R_Q = 120$ , and this choice implies a Clapeyron slope of  $6^\circ\text{C km}^{-1}$ . These parameters will result from a vertical temperature change of  $500^\circ\text{C}$ ,  $\Delta\rho = 0.08$ , and  $q_L = 40 \text{ cal g}^{-1}$  when  $g\alpha D^3/\kappa\nu = 1$ . These values for  $\Delta\rho$  and  $q_L$  are the values suggested by Schubert and Turcotte [1971] as typical of the olivine-spinel transition in the upper mantle. The effect of the phase change

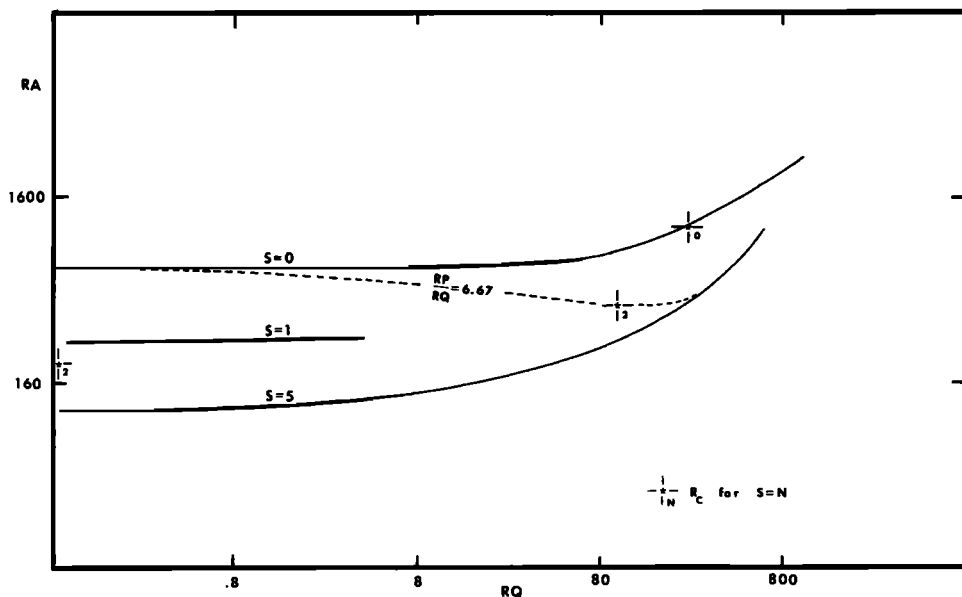


Fig. 18. Numerical critical Rayleigh numbers for three test cases and analytical neutral curves for convection through a phase boundary.

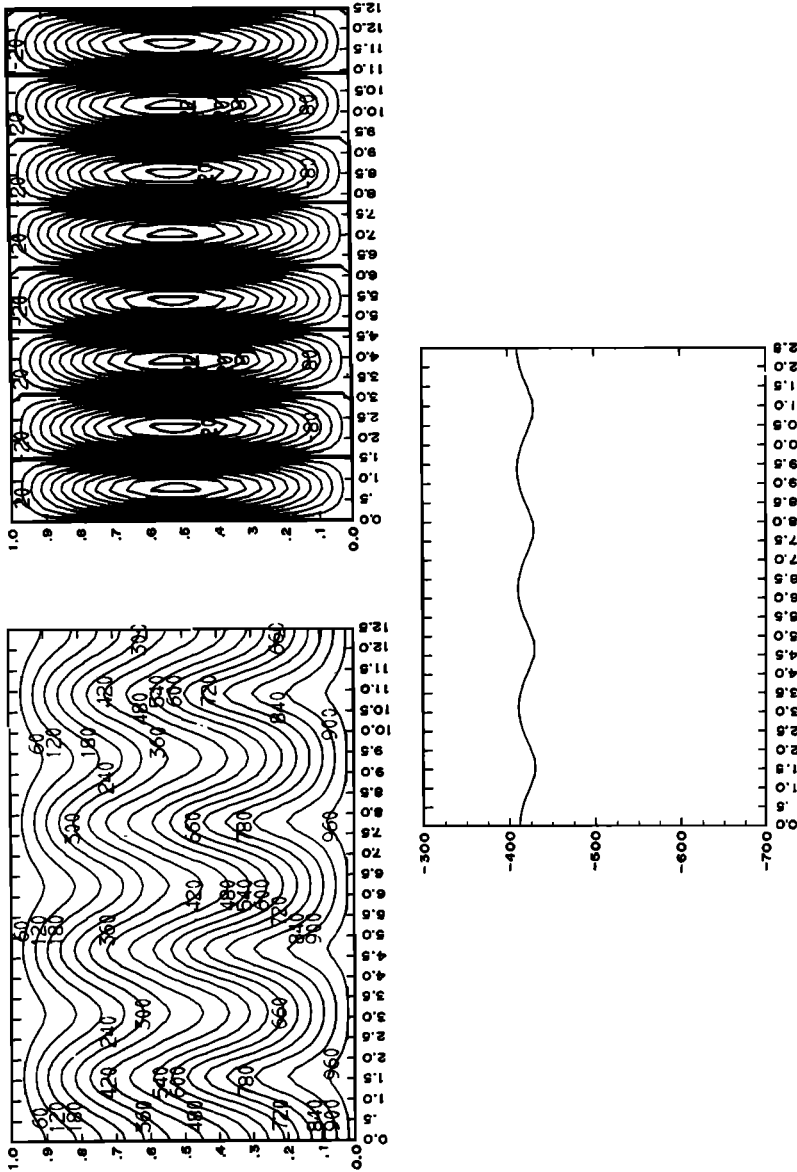


Fig. 19. Steady Rayleigh-Benard convection through a phase boundary having the properties of the olivine-spinel transition in the upper mantle;  $R_s = 500$ . Top left: temperature, contours from 0 to 0.96. Top right: stream function, contours from -2.2 to 2.2. Bottom: dimensional depth to phase boundary with  $D = 1000$  km.

is clearly destabilizing, since  $R_a = 500$  is subcritical in the absence of a phase change. The phase boundary ( $\Gamma = 0.5$  surface) has periodic changes in elevation that result from the horizontal variations of the temperature field. The phase boundary is at shallower depth in regions of down-welling, since the down-welling promotes locally cooler temperatures.

It is interesting to compare the amplitude of Rayleigh-Benard convection through a phase boundary to the amplitude of single-phase convection. Figure 20 shows the steady-state amplitude of both these cases as a function of the Rayleigh number. The parameter range was chosen to include a phase change having the properties of the olivine-spinel transition in the upper mantle. The effect of the phase change is to increase the amplitude of Rayleigh-Benard convection for all values of  $R_a$ .

The amplitude of steady Rayleigh-Benard convection in a single-phase system can be written in terms of the Rayleigh number as

$$A = C_1[(R_a - R_c)/R_c]^{1/2}$$

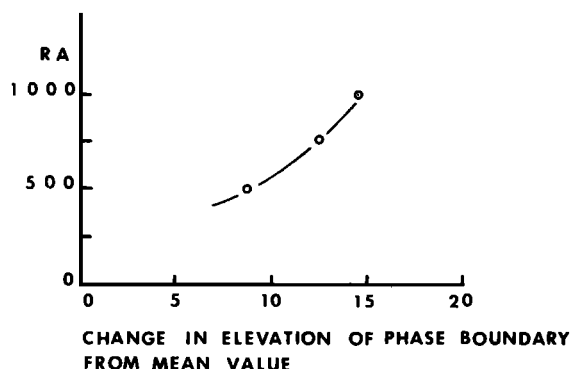
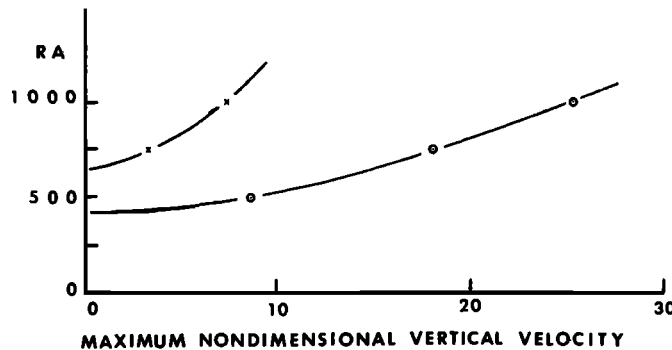


Fig. 20. Effect of a phase change on amplitude of Rayleigh-Benard convection and effect of convection on the elevation of the phase boundary. Dotted circle indicates  $R_a/R_c = 0.24$  and  $R_p/R_c = 6.67$ . Cross mark indicates  $R_a = 0$  and  $R_p = 0$ .

where

- $R_c$  the critical Rayleigh number;  $R_c = 657.5$ .  
 $C_1$  constant;  $C_1 = 10.88$ .

The amplitude data for convection through a phase boundary can be fitted by a similar relation if  $C_1 = 23$  and  $R_c = 450$ . This suggests that for Rayleigh numbers greater than 1000 the effect of the phase change will be to increase the amplitude by a factor of approximately 2.

Figure 20 also shows the effect of finite-amplitude convection on the elevation of the phase boundary for the same three cases shown in the upper graph. Therefore vertical velocities can be related to changes in phase boundary elevation. If the velocity is dimensionalized by using  $D = 1000$  km and  $\kappa = 10^{-2}$  cm<sup>2</sup> sec<sup>-1</sup>, then a vertical velocity of 0.1 cm yr<sup>-1</sup> results in approximately a 15-km change in the phase boundary elevation from its mean value.

Figure 21 shows the effect of changing the mean depth at which the phase change occurs. The mean depth of the phase change is  $0.75D$ . The variations in the phase boundary depth are no longer sinusoidal and show definite 'peaking' on the side away from the nearest boundary. Similar peaking away from the nearest boundary is found if the phase change is at shallow depth. No good explanation for this effect has been found.

Up to this point we have restricted our attention to phase changes with positive Clapeyron slopes. Ahrens and Syono [1967] suggest that the transformation of Mg<sub>2</sub>SiO<sub>4</sub> in the spinel structure to periclase and SiO<sub>2</sub> in the stishovite structure, which occurs at an average depth of 800 km, has a negative Clapeyron slope. A numerical calculation was performed by using their parameters for this reaction. The hope was that a phase change with negative slope would prove a barrier to vertical motions and thus provide a determinable lower boundary to the asthenosphere. The calculations showed that a phase change having the properties of the spinel-stishovite transition is mildly stabilizing (compared with no phase change), but it is not a barrier to vertical motions. Figure 22 shows the results for Rayleigh number 2000. The principal effect of the negative slope of the Clapeyron curve is that now the phase boundary is at shallower depth in regions of up-welling.

It is at first surprising to find that changing the slope of the Clapeyron curve from positive to negative has so little effect on flows through the phase boundary. This lack of dramatic effect can best be understood by considering the equation governing the system. The vorticity equation is

$$\nabla^2 \eta = R_a \partial T / \partial x - R_p \partial \Gamma / \partial x$$

If the Clapeyron curve has positive slope, then  $\partial T / \partial x$  and  $\partial \Gamma / \partial x$  have everywhere opposite sign, as can be seen in Figure 22. Therefore both these sources generate vorticity of the same sign. This implies that the term  $R_p \partial \Gamma / \partial x$  is destabilizing. On the other hand, cellular motions will cause heat to be released in regions of down-welling and absorbed in regions of up-welling. This has the effect of decreasing horizontal temperature gradients and thus degrades a source of vorticity. If the Clapeyron curve has negative slope, a similar line of reasoning leads one to conclude that the term  $R_p \partial \Gamma / \partial x$  is now a sink for vorticity generated by  $\partial T / \partial x$ ,

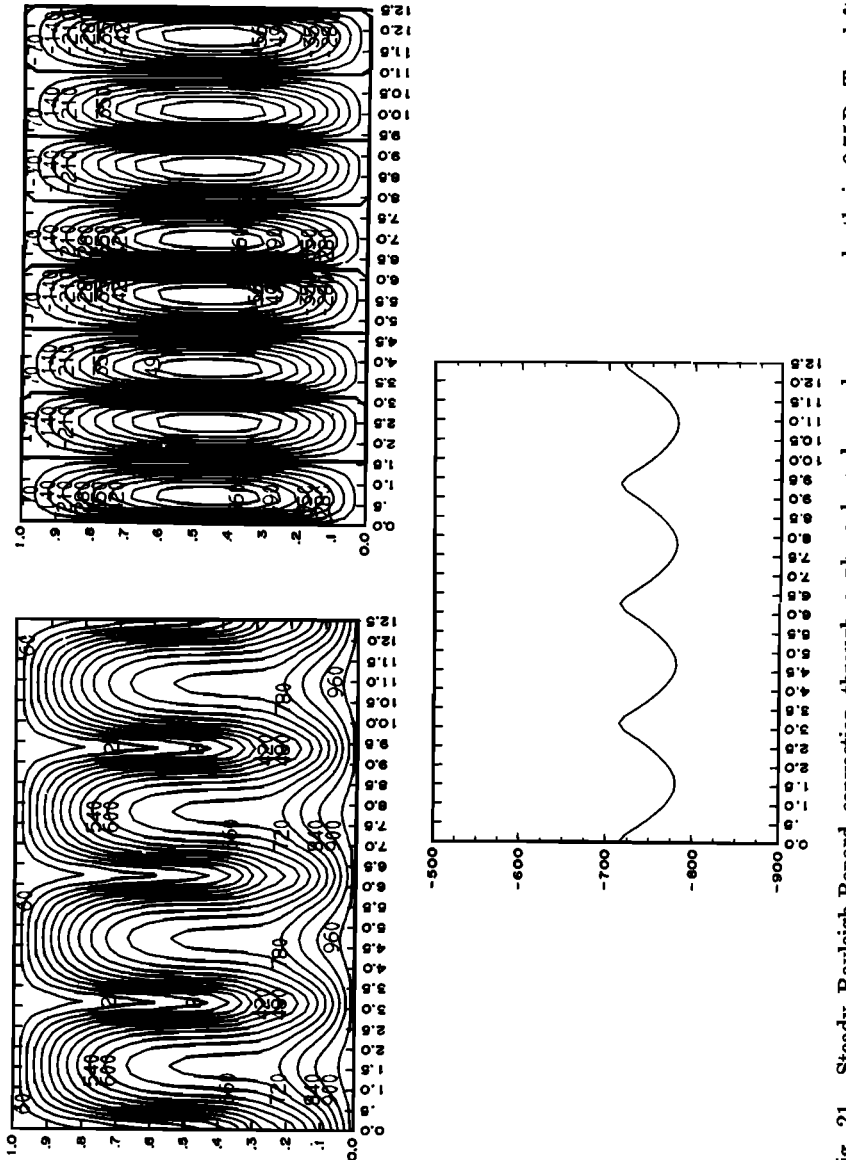


Fig. 21. Steady Rayleigh-Benard convection through a phase boundary whose mean depth is  $0.75D$ . Top left: temperature, contours from 0 to 0.96. Top right: stream function, contours from  $-5.6$  to  $5.6$ . Bottom: dimensional depth to phase boundary.  $R_a = 1000$ ,  $R_p = 8000$ ,  $R_q = 240$ ,  $\Delta T = 500^\circ\text{C}$ ,  $T_0 = 1200^\circ\text{C}$ , and  $D = 1000 \text{ km}$ .

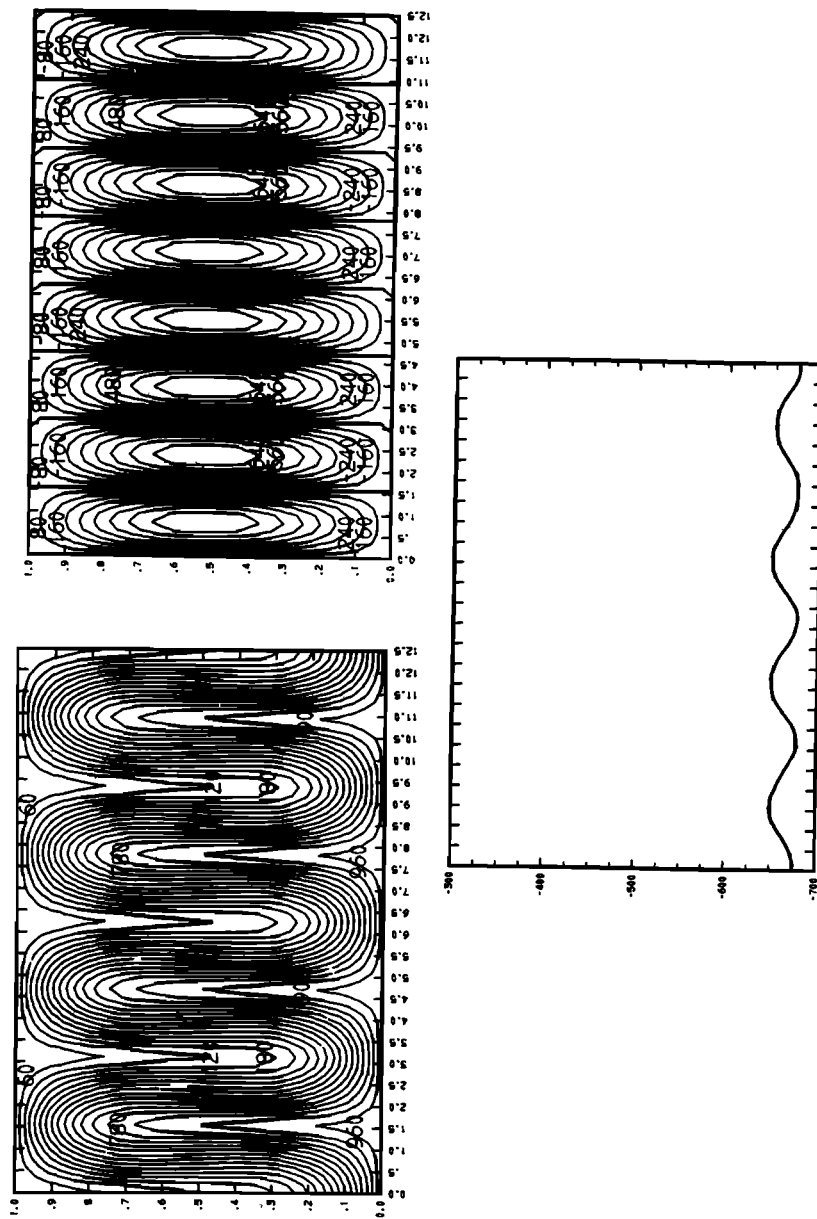


Fig. 22. Steady Rayleigh-Benard convection through a phase change having negative Clapeyron slope. Top left: temperature, contours from 0 to 0.96. Top right: stream function, contours from  $-6.4$  to  $6.4$ . Bottom: dimensional depth to phase boundary.  $R_s = 2000$ ,  $R_p = 18,000$ ,  $R_g = -60$ ,  $\Delta T = 500^\circ\text{C}$ ,  $T_0 = 1200^\circ\text{C}$ , and  $D = 1000$  km.

whereas the energy of phase change enhances the source  $\partial T/\partial x$ . The difference between the positive and negative Clapeyron slope cases is that the roles of the two opposing dynamical properties of the phase change are reversed.

The question of whether phase changes must be included in the formulation of subsequent model problems can now be considered. One of the principal dynamic effects of a phase change is to shift the critical Rayleigh number. This does not seem to be of great importance (to subsequent models) if we note that the amplitude of Rayleigh-Benard convection depends on the difference between the actual and the critical Rayleigh number and that the actual Rayleigh number in the upper mantle is not known within an order of magnitude. It is unnecessary to specify the critical Rayleigh number exactly when such uncertainty exists regarding the actual Rayleigh number. In the case of horizontal convection, phase changes (in the parameter range considered) increased the amplitude of the motion by a factor of 3. A potential error of a factor of 3 cannot be very important if we do not know the proper value ( $\kappa/D$ ) to use in redimensionalizing the model velocities. The final point is that, although phase changes may effect the amplitude, they have very little effect on the structure of the flow. The overall conclusion is that until we have better estimates of the parameters pertinent to asthenosphere motions, the dynamic effect of phase changes can be ignored in the subsequent model problems.

Once models of particular geophysical interest are found, it may be useful to include phase changes as a second step. We would include the phase changes, not so much because of their effect on the motions, but rather to estimate the effect of the motions on the phase boundary elevation. Changes in phase boundary elevation may be detectable by geophysical techniques [Julian, 1970] and thus could provide a way of testing the validity of any given model.

## 6. LITHOSPHERE-ASTHENOSPHERE MODELS

All the previous model problems treat the asthenosphere as separable from the lithosphere. These problems were sufficient to answer specific questions about possible flows in the asthenosphere but cannot be thought of as dynamic models of sea floor spreading. The complete dynamics of present-day sea floor spreading can only be studied by using coupled lithosphere-asthenosphere models for the following reasons: (1) the motion of a lithospheric plate is a very strong source of vorticity; (2) a moving lithosphere implies a net mass flux in the asthenosphere from trench to ridge; and (3) the subduction of lithospheric material into the asthenosphere results in dynamically significant temperature and density variations.

In this section we shall investigate two lithosphere-asthenosphere models that reflect the geometry shown in Figure 2. The first model considers the left half of the figure and accordingly is called the Pacific model. The second model (Atlantic model) reflects the geometry of the right half of Figure 2.

a. *Pacific model.* The geometry and nondimensional boundary conditions of the Pacific model are shown in Figure 23.

The portion of the figure marked by diagonal lines represents the lithosphere

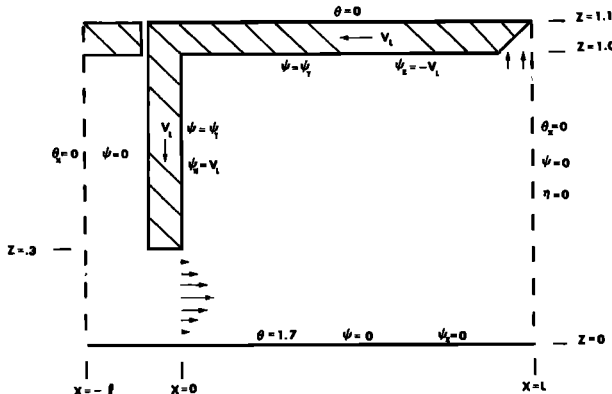


Fig. 23. Pacific model.

with a ridge at  $x = L$  and a subduction zone at  $x = 0$ . The geometry of the model is considered to be unchanging even when the lithosphere moves ( $V_L \neq 0$ ), because material is continuously added to the plate at the ridge ( $x = L$ ) and is lost at depth under the trench ( $x = 0$ ). We are ignoring changes in geometry that result from the migration of the site of subduction, the philosophy being that if we can find a viable model that does not depend in any important way on the exact geometry, the model will be valid even if the geometry is changing slowly.

The temperature boundary conditions are applied to a larger domain ( $-l \leq x \leq L$ ,  $0 \leq z \leq 1.1$ ) than are the kinematic and dynamic boundary conditions ( $0 \leq x \leq L$ ,  $0 \leq z \leq 1.0$ ). The temperature boundary condition at  $x = -l$  and  $x = L$  results from assuming the model to have geometric symmetry about  $x = -l$  and  $x = L$ . The lithosphere contains heat sources such that  $\theta = 1.2$  at  $z = 1$ . If we dimensionalize the temperature by using  $\Delta T = 1000^\circ\text{C}$ , this would result in a geophysically reasonable temperature of  $1200^\circ\text{C}$  at the base of the lithosphere.

The dynamic and kinematic boundary conditions, shown in Figure 23 in terms of the vorticity  $\eta$  and stream function  $\psi$ , have the following physical interpretation. At  $z = 1.0$  the fluid must move with the velocity of the overlying plate, and therefore  $\psi_z = -V_L$ . The condition  $\psi = \psi_T$ , a constant, comes from requiring that the horizontal mass flux in the asthenosphere balance the mass flux implied by  $V_L$ . If we choose  $\psi = 0$  at  $z = 0$ , then mass conservation requires

$$\int_0^{1.1} \psi_z dz = \int_0^1 \psi_z dz + \int_1^{1.1} \psi_z dz = 0$$

which, when evaluated, results in  $\psi_T = 0.1V_L$ . Similarly, the boundary conditions at  $x = 0$ ,  $0.3 < z < 1.0$  require that the fluid move with velocity  $V_L$ . The boundary  $z = 0$  is not moving, and thus fluid velocities must vanish there, which can be specified by requiring that  $\psi$  and  $\psi_z$  be 0. The condition  $\psi = 0$  and  $\eta = 0$  on  $x = L$  result from the geometric symmetry of the problem about  $x = L$ . The boundary conditions on the asthenosphere are completed by specifying an influx of mass at  $x = 0$ ,  $0 < z < 0.3$  and an outflow at the ridge ( $x = L$ ). The velocity profile at  $x = 0$  was chosen to have the vertical structure of a  $\text{sech}^2$  centered at

$z = 0.15$ . The outflow profile is taken to be constant. A final condition is imposed by requiring that  $\psi = 0$  for  $x < 0$ . This condition implies only that we are ignoring the advection of heat in the region to the left of the downgoing slab. If we can find a way to specify  $V_L$ , we need only calculate  $\psi$  and  $\eta$  over a simple rectangular domain  $0 \leq x \leq L$  and  $0 \leq z \leq 1.0$ .

The velocity of the lithosphere, if steady, results from a balance between the viscous stresses on the plate and any external forces acting on it. Several authors [McKenzie, 1969; Turcotte and Schubert, 1971] have indicated that the subducted lithosphere is denser than the material it penetrates and is therefore subjected to a negative buoyancy force. The balance of forces on the lithospheric plate can be written:

$$\int_L^0 \sigma_x dx + \int_1^{0.3} \sigma_z dz = F_g \quad (53)$$

where  $\sigma_x$  and  $\sigma_z$  are the viscous stresses on the plate and  $F_g$  is the total negative buoyancy force. In principle, the negative buoyancy force can be determined by using the temperature field solution calculated. However, it is preferable to use the values reported by Turcotte and Schubert, since their analysis of the thermal regime of the downgoing slab is much more sophisticated than the present more general formulation permits.

One approach to the model problem is to prescribe  $V_L$ , calculate the stresses, and then use (53) to find the negative buoyancy force required to maintain the prescribed  $V_L$ . The required buoyancy can be compared to the reported values to find if a viable model results. Using this approach, numerical solutions were obtained for various values of  $V_L$ .

Figure 24 shows the nondimensional temperature and stream function field for a case in which  $R_o = 10^4$  and  $V_L = 300$ . A nondimensional velocity of 300 corresponds to a dimensional plate velocity of  $1 \text{ cm yr}^{-1}$  if  $\kappa = 10^{-2} \text{ cm}^2 \text{ sec}^{-1}$  and  $D = 1000 \text{ km}$ . When these values of  $\kappa$  and  $D$  are used, the figure represents a dimensional time of  $7 \times 10^7$  years after the beginning of subduction.

The temperature field was allowed to reach a steady state before the velocity boundary conditions were imposed. Once motions begin, the isotherms are warped by the downgoing slab. The fluid to the left of the slab is quiescent, whereas the fluid on the right must satisfy a no-slip boundary condition. By comparing the temperatures on either side of the slab, one concludes that the effect of advection in the surrounding asthenosphere is to reduce horizontal temperature gradients near the slab.

The stream function field is more complicated than expected. The large-scale flow is a vortex, driven primarily by the moving boundaries, whose center is well above the midpoint of the fluid layer. A smaller region of closed circulation can be seen near the downgoing slab. These characteristics of the flow persisted even in cases where the Rayleigh number was as small as 1, which indicates that they must be properties of the solution of the biharmonic equation  $\nabla^4\psi = 0$ .

Pan and Acrivos [1966] have solved the biharmonic for low Reynolds number, steady flow in a rectangular cavity where the motion is driven by the uniform translation of a boundary. They find that the structure of the flow is very

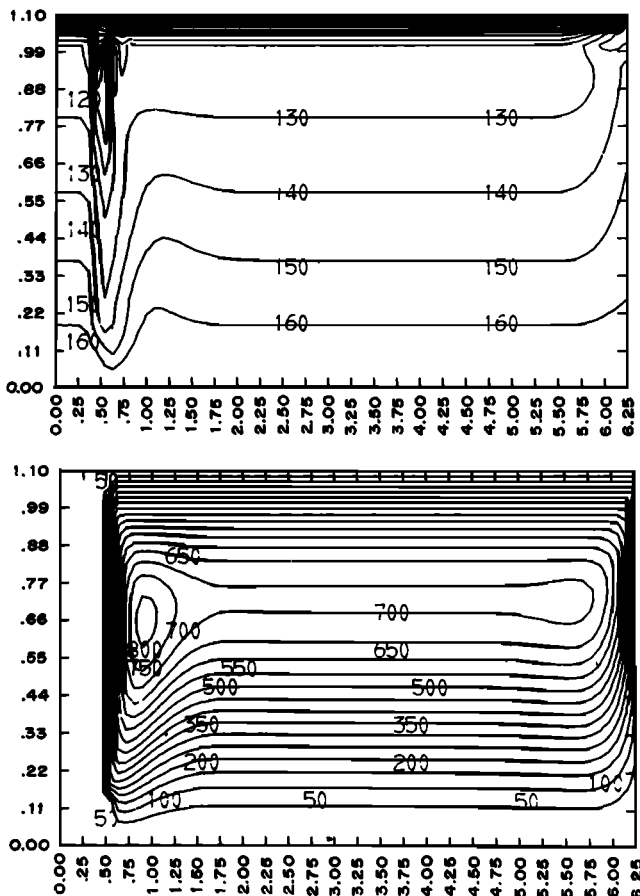


Fig. 24. Pacific model with  $R_e = 10^4$ ,  $V_L = 300$  ( $1 \text{ cm yr}^{-1}$ ) and time = 0.01045 ( $\approx 7 \times 10^7$  yrs) after subduction begins. Top: temperature contours from 0 to 1.60. Bottom: stream function, contours from 0 to 80.0.

dependent on the aspect ratio of the cavity. The shallowest layer they consider has an aspect ratio  $D/L$  of 0.25 (Figure 24 has an aspect ratio of approximately 0.15). For the shallowest case, they find that the center of the large vortex is centered at  $D/3$ . Figure 25a, taken from their paper, shows this result. If the flow in the cavity is driven by its shorter boundary, a primary cell of aspect ratio 1 develops near the moving boundary. Weaker cells fill the rest of the domain, but their amplitude is smaller by a factor of  $10^4$  (Figure 25e). Since the biharmonic operator is linear, we can superimpose flows 25a, e. Such a superposition confirms the general characteristics of the flow in Figure 24.

Having gained a measure of confidence in our solution, we can consider the question of the negative buoyancy required to move a lithospheric plate at geophysically reasonable rates. If the plate is moving with constant velocity, the total viscous drag exerted by the fluid below is a measure of the negative buoyancy of the downgoing slab (equation 53). Figure 26 summarizes the results

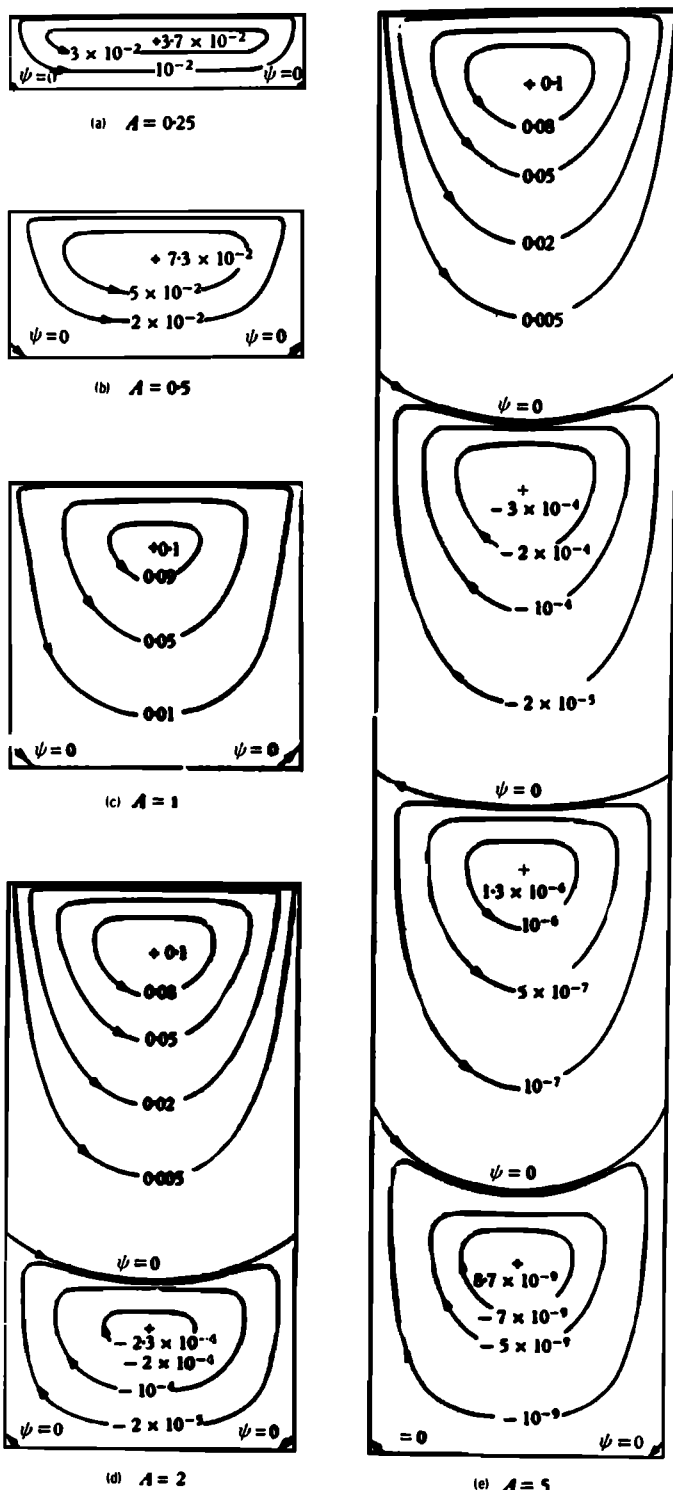


Fig. 25.

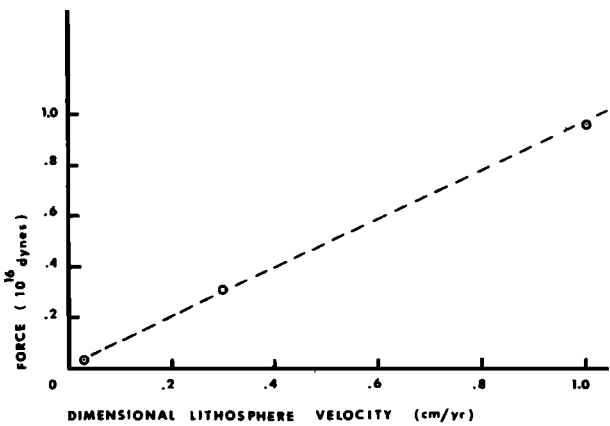


Fig. 26. Lithosphere velocity as a function of total negative buoyancy of subducted slab from Pacific model with  $R_s = 10^4$ .

of three numerical calculations and shows the buoyancy force required to maintain a given plate velocity. The total force and velocity have been dimensionalized using  $\kappa = 10^{-2} \text{ cm}^2 \text{ sec}^{-1}$ ,  $D = 1000 \text{ km}$ , and  $\mu = 10^{22} \text{ poises}$ . The published estimates of total negative buoyancy [McKenzie, 1969; Turcotte and Schubert, 1971] are in the range  $10^{16}$ - $10^{17}$  dynes. These estimates result in model spreading velocities in the range  $1$ - $10 \text{ cm yr}^{-1}$ , which is the range of observed spreading rates. The agreement in plate velocity between this model and observations does depend on the value of the physical quantities used in dimensionalizing the velocity, and, as previously pointed out, these quantities are not known exactly. Keeping this note of caution in mind, the principal conclusions derived from this model problem are that (1) the moving plates are themselves an important source of vorticity and drive a large primary vortex with a smaller region of closed circulation near the downgoing slab, and (2) the negative buoyancy is always an important dynamical quantity and is sufficient to explain observed spreading rates if present estimates of the physical quantities involved are correct.

The implicit assumption is made that the negative buoyancy force can be transmitted to the overlying lithosphere. What happens if the downgoing slab is not mechanically coupled to the overlying lithospheric plate? Since this mechanical decoupling is true for plates bordering the Atlantic ridge (Figure 2), we proceed to investigate what I have called the Atlantic model.

b. *Atlantic model.* The formulation of the Atlantic model differs from formulation of the Pacific model in two ways. First, since the overlying lithosphere is no longer directly coupled to the downgoing slab, the balance of forces on the lithosphere becomes simply

$$\int_L^0 \sigma_x dx = 0 \quad (54)$$

Fig. 25. (Opposite) Solution of the biharmonic equation in a rectangle with uniform translation of one boundary [after Pan and Acrivos, 1967].  $A$  is aspect ratio defined as depth over width.

when  $V_L$  is constant. The second difference is that the heat sources within the lithosphere have been redistributed to simulate the thermal effect of the continent embedded in the Atlantic plate. Aside from these two changes, the model is the same as the one shown in Figure 23.

The model problem is to be solved numerically. We can no longer specify  $V_L$  a priori, as we could in the Pacific model, since there are no external forces on the plate besides the viscous stresses. The velocity of the plate is found using a relaxation technique that varies  $V_L$  until the stress constraint (54) is satisfied to a prescribed accuracy. Such a procedure is convergent but costly, since for every new value of  $V_L$  in the iteration a new interior flow must be calculated ( $V_L$  is a boundary condition on the interior flow). This method for finding  $V_L$  is formally valid only if  $V_L$  is constant with time. However, since the overlying plate will respond almost instantaneously to changes in the interior flow (the time scale being inversely proportional to the viscosity), the method will be used even when  $V_L$  is a slowly varying function of time.

Figure 23 assumes that the velocity of the downgoing slab is equal to the velocity of the lithospheric plate. In the physical problem that motivates this figure, the rate of subduction depends on the sum of the velocity of the two plates converging at the trench. Therefore we can also consider cases where the rate of subduction is greater than the velocity of the Atlantic plate alone.

The first question we can consider using the Atlantic model is the efficiency of a single convective cell in moving an overlying plate. A series of numerical experiments with a single cell driven by horizontal temperature variations on the boundaries were calculated. The results indicate that a single cell generates a plate velocity approximately equal to the maximum cell velocity multiplied by the ratio of the width of the cell to the length of the overlying plate. We thus have a 'rule of thumb' that states:

$$V_L = U_{\max} (H/L) \quad (55)$$

where

$U_{\max}$  maximum cell velocity.

$H$  width of cell.

$L$  length of the overlying plate.

Furthermore, since the integral constraint used to find  $V_L$  is independent of viscosity, the rule of thumb is also independent of viscosity.

Figure 27 is an example of the Atlantic model in which the Rayleigh number is  $10^4$  and the rate of subduction equals  $V_L$ . The lithosphere contains a continent extending from the subduction zone at  $x = 0.6$  to  $x = 5$ . In the early stages of spin-up (Figure 27a), the edge cell at  $x = 5$ , driven by the thermal presence of the continent, is the dominant feature of the flow. The nondimensional velocity of the overlying plate (-2.0) is approximately  $1/3U_{\max}$ , as the rule of thumb would suggest. At a later stage (Figure 27b), Rayleigh-Benard cells have reached significant amplitude, and their effect is to slow the plate and eventually bring it to rest. The variation in cell size is due to the many mechanisms present in the model that can add to or detract from Rayleigh-Benard convection.

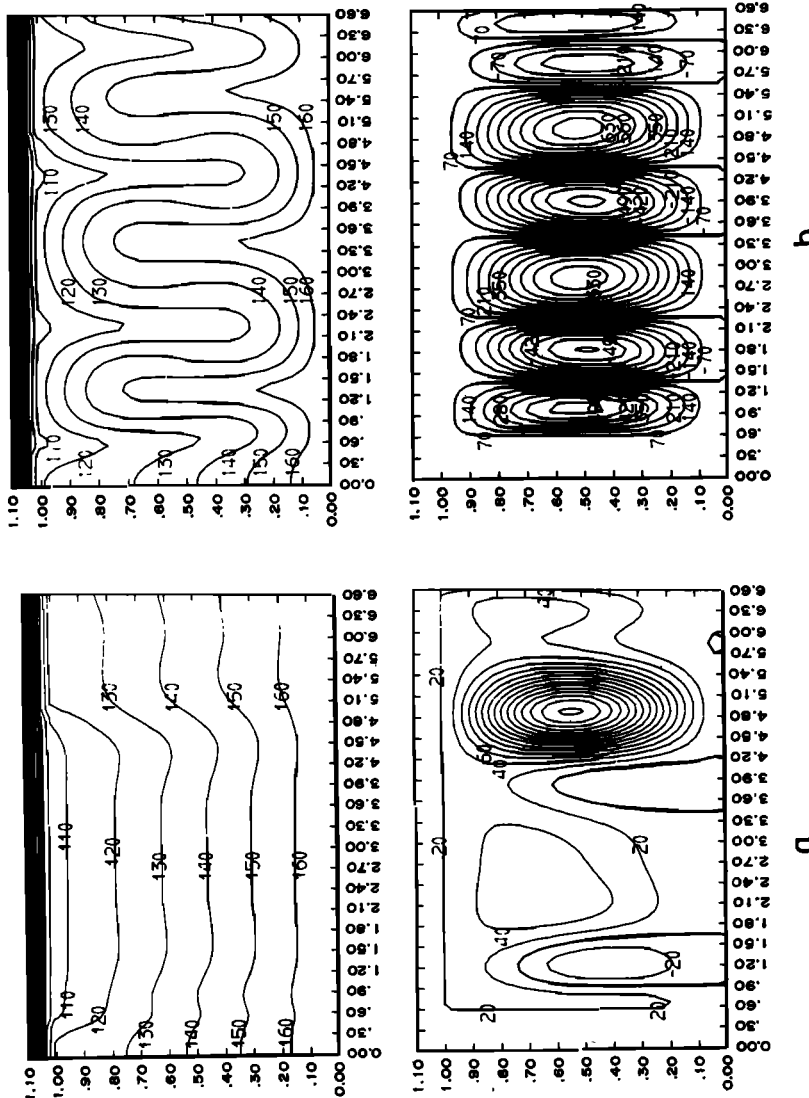


Fig. 27. Atlantic model with  $R_a = 10^4$ . (a) Early stages of spin-up ( $V_L = 10^{-1} \text{ cm yr}^{-1}$ ). Top left: temperature, contours from 0 to 1.60. Bottom left: stream function, contours from -0.2 to 3.0; (b) later stage ( $V_L = 10^{-4} \text{ cm yr}^{-1}$ ) later stage ( $V_L = 10^{-4} \text{ cm yr}^{-1}$ ). Top right: temperature, contours from -5.6 to 6.3.

Even with the Rayleigh number equal to  $10^4$ , the maximum dimensional plate velocity reached was only  $10^{-2}$  cm yr<sup>-1</sup> (where  $\kappa = 10^{-2}$  cm sec<sup>-1</sup> and  $D = 1000$  km). The conclusion drawn from this case and similar cases with different aspect ratios is that only small velocities are achieved if the plates are driven solely by the viscous traction of thermally driven flows. The fact that the Rayleigh-Benard cells can overcome the edge cell has been seen before in connection with the breakup problem.

Fortunately, we still have the freedom of considering models in which the rate of subduction is greater than the velocity of the overlying plate. Figure 28 represents the same calculation as Figure 27, only that now the rate of subduction is  $3V_L$ . The resulting plate velocity is greater and the Rayleigh-Benard cells no longer bring the plate to rest. The effect of the rate of subduction can be seen in Figure 29, in which the plate velocity as a function of time is shown

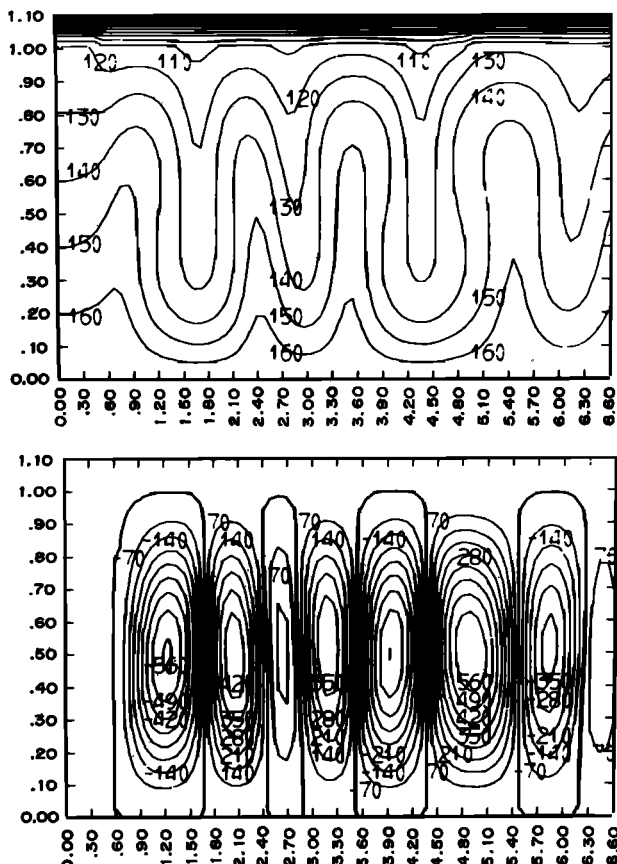


Fig. 28. Atlantic model with  $R_s = 10^4$ . Same case as Figure 27b except that subduction rate is  $3V_L$  (with  $V_L \approx 10^{-2}$  cm yr $^{-1}$ ). Top: temperature, contours from 0 to 1.60. Bottom: stream function, contours from -5.6 to 5.6.

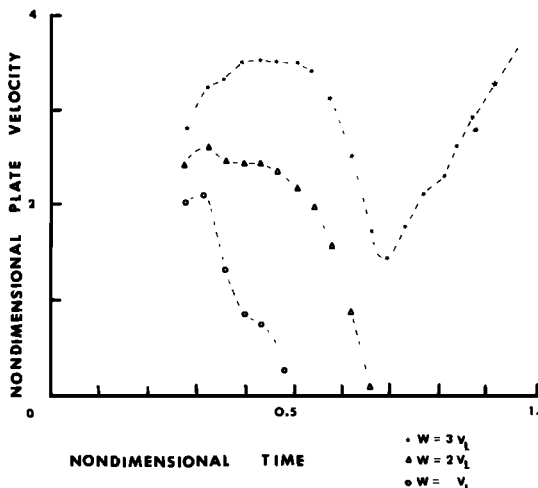


Fig. 29. Nondimensional lithosphere spreading velocity as a function of time for three subduction rates  $W$ . The curves  $W = V_L$  and  $W = 3V_L$  include the cases shown in Figures 27 and 28.

for various rates of subduction  $W$ . The velocity of the lithosphere grows initially as the edge cell spins up. As Rayleigh-Benard cells reach significant amplitude, the plate velocity begins to decrease. If the rate of subduction is sufficiently large, it begins to bias the Rayleigh-Benard cells in such a way that the plate velocity begins to increase again.

Figure 30 is a better illustration of the role of the downgoing slab as a modifier of Rayleigh-Benard cells. The aspect ratio in this case is about 0.3; this enhances the effect of the slab, which is being subducted at a rate of  $2V_L$ . The rate of subduction is sufficiently large in this case to virtually destroy the Rayleigh-Benard cells. The dimensional velocity in this example is  $0.1 \text{ cm yr}^{-1}$ .

These Atlantic models suggest that convection, either in the Rayleigh-Benard sense or driven by horizontal temperature gradients of the order of  $100^\circ\text{C}/1000 \text{ km}$ , is a relatively inefficient mechanism for driving an overlying plate. Furthermore, if the models include significantly large (but geophysically reasonable) lithospheric velocities, it appears that cellular convection is no longer a physically realizable flow. This suggests that the role of the downgoing slab, even when not directly coupled to the overlying lithosphere, is essential in obtaining reasonable plate velocities.

The effect of a decoupled downgoing slab can be estimated by using a different approach. Let us assume for the moment a subduction rate of  $V_s$ . The calculation of Pan and Arivos (Figure 24) tells us that a cell of aspect ratio 1 results. Then, by using the rule of thumb (55), we find that the lithospheric plate, even though decoupled, will move with a velocity  $V_L = V_s(D/L)$ , where  $D$  is the depth extent of the asthenosphere, and  $L$  is the distance from trench to ridge. This result implies that, even when not mechanically coupled to a lithospheric plate, the downgoing slab can generate velocities of the order of  $1 \text{ cm yr}^{-1}$ .

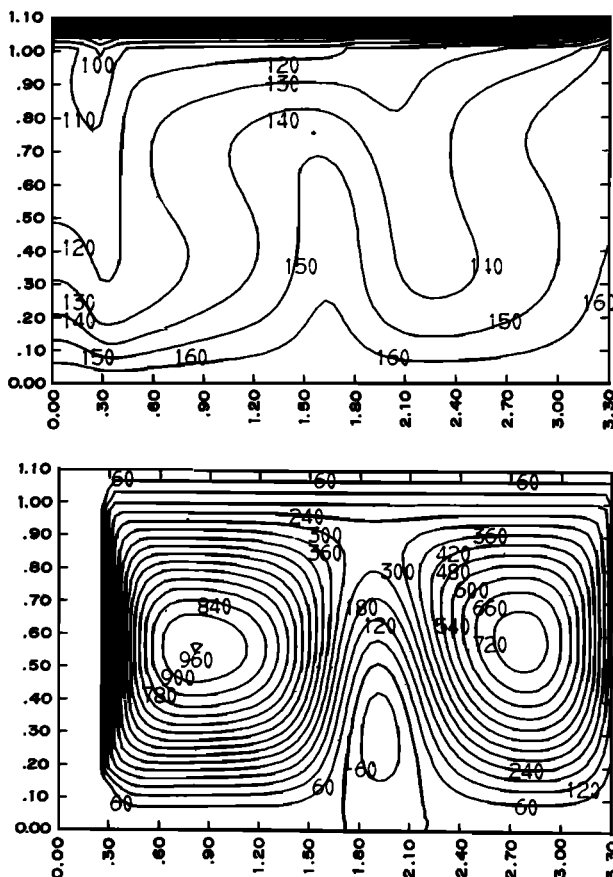


Fig. 30. Atlantic model in late stages of spin-up with  $R_s = 10^4$  and subduction rate of  $2V_L$  (with  $V_L \approx 10^{-1}$  cm yr $^{-1}$ ). Top: temperature, contours from 0 to 1.6. Bottom: stream function, contours from -0.6 to 9.6.

## 7. CONCLUSIONS

The three principal requirements of a dynamical model of sea floor spreading are given below.

1. The model must generate net forces on the lithosphere capable of first breaking it and must then transport the resulting fragments away from the original fracture.
2. Once the lithosphere begins to move away from the fracture, the asthenosphere must balance the mass flux implied by this motion.
3. These first two requirements must be satisfied in a length of time, the most upper bound of which is the age of the earth.

In terms of these requirements, the most important conclusions derived from the various model problems are restated below.

**Rayleigh-Benard convection:**

1. Generates periodic stresses and thus no net force on an overlying plate.
2. Does not satisfy the required mass transport in the asthenosphere from trench to ridge.

**Combined horizontal and Rayleigh-Benard convection:**

1. Can provide a net force on an overlying plate.
2. Suggests a break-up mechanism for large continental masses, in relation to which smaller continents are stable.
3. Does not satisfy required mass transport in the asthenosphere.

**Phase changes:**

1. Can increase or decrease critical Rayleigh number of Rayleigh-Benard convection.
2. Can increase or decrease finite amplitudes by a numerical factor of the order of one. The olivine-spinel transition increases the amplitude of convection by a factor of about two.
3. Do not affect the structure of the flow.
4. Vary in depth owing to advected heat, and these variations may provide a viable test of kinematic models of the asthenosphere.

**Pacific model:**

1. Produces lithospheric velocities of the same order as geophysically interpreted plate velocities.
2. Satisfies mass transport requirement in the asthenosphere.
3. Has growth time very short compared to the age of the earth.

**Atlantic model:**

1. Produces only small plate velocities if the lithosphere is driven solely by thermally generated flows.
2. Is such that sufficiently large and consistent plate velocities result if the rate of subduction of a mechanically decoupled (from Atlantic plate) down-going slab is greater than the Atlantic plate velocity itself.
3. Satisfies mass transport requirement in the asthenosphere.
4. Has growth time short compared with age of the earth.

The most important dynamical conclusion derived from the sequence of model problems is the preeminence of the subducted lithosphere among the driving mechanisms considered. The downgoing slab, by virtue of its large negative buoyancy, is capable of directly driving the Pacific plate and indirectly driving the Atlantic plate at geophysically reasonable velocities. Even if the negative buoyancy has been exaggerated, a moving lithosphere and downgoing slab impose velocity boundary conditions that cannot be ignored in any discussion of flows in the asthenosphere.

The complete set of model problems are suggestive of the following sequence of events. A major continental mass is fractured by the viscous traction, on the base of the lithosphere, of thermally driven flows. Since this mechanism is found to be incapable of generating large plate velocities, the fracture need not lead

to significant spreading. The widespread existence of continental scale rifting throughout the geologic record may be evidence of frustrated spreading attempts. If, on the other hand, the thermally driven spreading exceeds a critical length, subduction of the lithosphere begins, and a new element enters the dynamics of the system. This second stage, driven primarily by the negative buoyancy of the downgoing slab, is both fast ( $1\text{--}10 \text{ cm yr}^{-1}$ ) and irreversible. This stage also implies that plates supplying the subducted material move fastest. This sequence of events is really just the gravitational instability of lithospheric plates to finite amplitude perturbations provided by thermally driven flows.

#### APPENDIX: NUMERICAL FORMULATION OF MODEL PROBLEMS

The most general set of nondimensional equations that we encounter are those governing a two-phase system. They are

$$\partial\theta/\partial t = J(\psi, \theta - R_q/R_a\Gamma) + R_q/R_a \partial\Gamma/\partial t + \nabla^2\theta \quad (56)$$

$$\nabla^2\eta = R_a \partial T/\partial x - R_p \partial\Gamma/\partial x \quad (57)$$

$$\nabla^2\psi = \eta \quad (58)$$

where

$\theta$  temperature.

$\eta$  vorticity.

$\psi$  stream function.

$\Gamma$  fractional concentration of denser phase.

$R_a$  Rayleigh number based on typical temperature scale;  $R_a = g\alpha\Delta TD^3/\kappa\nu$ .

$R_p$  Rayleigh number based on fractional change in density between the two phases ( $\Delta\rho$ );  $R_p = g\Delta\rho D^3/\kappa\nu$ .

$R_q$  Rayleigh number based on energy released per unit mass of material changing phase ( $q_L$ );  $R_q = g\alpha(q_L/C_p)D^3/\kappa\nu$ .

The effect of the phase change can be suppressed by choosing  $R_p = 0$  and  $R_q = 0$ .

The most general boundary conditions, in terms of a normal coordinate  $\xi$  and a tangential coordinate  $\zeta$ , are  $T_{\xi=0} = T_{(\xi)}$ ;  $\psi_{\xi=0} = \psi_{(\xi)}$ , which specifies the velocity normal to the boundary; and  $\partial\psi/\partial\xi_{\xi=0} = \Phi_{(\xi)}$ , which specifies the velocity along the boundary.

The temperature equation can be integrated by using the explicit scheme of *Dufort and Frankel* [1953]. The finite difference analogue to (56) becomes

$$\begin{aligned} \frac{\theta_{i,j}^{n+1} - \theta_{i,j}^{n-1}}{2\Delta t} &= J_A(\psi^n, \theta^n - R_q/R_a\Gamma^n) + R_q/R_a \frac{(\Gamma_{i,i}^n - \Gamma_{i,i}^{n-1})}{\Delta t} \\ &\quad + (1/\Delta x)^2(\theta_{i+1,i}^n + \theta_{i-1,i}^n - \theta_{i,i}^{n+1} - \theta_{i,i}^{n-1}) \\ &\quad + (1/\Delta z)^2(\theta_{i,i+1}^n + \theta_{i,i-1}^n - \theta_{i,i}^{n+1} - \theta_{i,i}^{n-1}) \end{aligned} \quad (59)$$

where  $n$  measures the time step and the subscripts  $i$  and  $j$  are the  $x$  and  $z$  grid points, respectively. We write  $J_A(\alpha, \beta)$ , the Jacobian operator, using the *Arakawa* [1966] scheme, which conserves  $\alpha$ ,  $\alpha^2$ ,  $\beta$ , and  $\beta^2$ .

To find  $\theta_{i,j}^{n+1}$ , we need  $\Gamma_{i,j}^n$ . We assume that the phase boundary corresponds

to the surface  $\Gamma = 0.5$  (50% concentration of each phase). The depth to the phase boundary ( $Z_{0i}$ ) at each  $x$  distance is defined by the intersection of the Clapeyron curve, written in temperature depth coordinates, and the local temperature gradient. The intersection of these two curves can be found by using any standard technique. Once we find  $Z_{0i}^n$ , we specify  $\Gamma_{i,j}^n$  as

$$\Gamma_{i,j}^n = 0.5[1 + \tanh(Z_{0i}^n - j(\Delta z)L)] \quad (60)$$

The vertical structure of  $\Gamma$  was specified to be a hyperbolic tangent centered at  $Z_{0i}$  and varying on a vertical length scale  $L$ . The effect of the arbitrariness in our choice of vertical structure is discussed in the section on the role of phase changes. It was found that as long as  $L$  is small compared with the depth of the fluid, the exact vertical structure of  $\Gamma$  is of no consequence. Having defined  $\Gamma_{i,j}^n$ , we can find  $\theta_{i,j}^{n+1}$  from (59).

The numerical, advective stability condition requires that  $\Delta t$ , the time step, satisfy  $U_m \Delta t / \delta < 1$ , where  $U_m$  is the maximum velocity and  $\delta$  the grid spacing. Even though the Dufort-Frankel scheme does not explicitly require it, I found that it is best to also satisfy a diffusive stability condition,  $\Delta t < \delta^2$ .

Once we have the updated ( $n + 1$ ) temperature field,  $\Gamma$  can be updated, and thus the source terms in the vorticity equations are determined. Both the vorticity equation (57) and the stream function equation (58) are Poisson equations, which are solved by using a noniterative scheme developed by Buneman [1969].

If we consider stress-free boundaries, the vorticity is 0 everywhere on the boundaries, and (57) and (58) can be solved directly. If we consider the more general case of moving, 'rigid' boundaries, the kinematic and dynamic boundary conditions are specified in terms of the stream function alone. There is no direct way in which the dynamic boundary condition  $(\partial \psi / \partial \zeta)_{\zeta=0} = \Phi_{(t)}$  can be transformed into a condition on the vorticity. This becomes clear if we consider that the vorticity is proportional to the stress on the boundary, and the stress is unknown until we actually solve the problem.

An iterative method, suggested by Israeli [1970], is used to obtain the vorticity on the boundaries consistent with the dynamic boundary condition on the stream function. The general iteration formula is

$$\eta_{i,0}^{K+1} = \eta_{i,0}^K + \omega \left[ \left( \frac{\partial \psi}{\partial \zeta} \right)_{i,0}^K - \Phi_i \right] \quad (61)$$

where the boundary is at  $j = 0$ ,  $K$  is an iteration counter, and  $\omega$  is a convergence parameter chosen by trial and error.

The normal derivative of the stream function on the boundary can be written in finite difference form as

$$(3/\Delta Z) \partial \psi^K / \partial \zeta_{i,0} = \frac{(8\psi_{i,1}^K - \psi_{i,2}^K - 7\psi_{i,0}^K)}{2(\Delta Z)^2} \quad (62)$$

Substitution of (62) into (61) yields

$$\eta_{i,0}^{K+1} = w\eta_{i,0}^K + (1-w) \left[ \frac{(8\psi_{i,1}^K - \psi_{i,2}^K - 7\psi_{i,0}^K)}{2(\Delta Z)^2} - 3\Phi_i / \Delta Z \right] \quad (63)$$

when  $\omega = (3/\Delta Z)(1-w)$ .

The iteration formula (63) requires an initial 'guess' of  $\eta_{i,0}^K$  and the value of the vorticity from the previous time step is the best guess available. The iteration in  $K$  requires that we solve both the vorticity and stream function equations for each  $K$ . Once  $\eta_{i,0}^{K+1} = \eta_{i,0}^K \pm E$  for  $E \ll 1$ , then the dynamic boundary condition is satisfied to an accuracy of  $\pm E/\omega$  (see equation 61).

The overall accuracy of the numerical scheme for solving equations (56) through (58) is best estimated by comparing the numerical results with analytical results. Such comparisons are made throughout this study.

*Acknowledgments.* I am indebted to Dr. J. Pedlosky for his guidance throughout the course of this work. Dr. M. Israeli made a vital contribution in suggesting the numerical technique that provides the vorticity on the boundaries.

This work, carried out at the University of Chicago, was supported under NSF grants GA-11951 and GA-28427. The final manuscript was completed while the author was at M.I.T., supported under N.S.F. grant GA-29358. Acknowledgment is made to the National Center for Atmospheric Research, which is sponsored by the National Science Foundation, for computer time used in this research.

#### REFERENCES

- Ahrens, T. J., and Y. Syono, Calculated mineral reactions in the earth's mantle, *J. Geophys. Res.*, 72, 4181, 1967.
- Allan, D. W., W. B. Thompson, and N. O. Weiss, Convection in the earth's mantle, in *Mantle of the Earth and Terrestrial Planets*, edited by S. K. Runcorn, p. 507, Interscience, New York, 1967.
- Anderson, D. L., Petrology of the mantle, *Mineral. Soc. Amer. Spec. Pap.* 3, 85, 1970.
- Arakawa, A., Computational design of long-term numerical integration of equations of fluid motions: Two-dimensional incompressible flow, 1, *J. Comput. Phys.*, 1, 119, 1966.
- Artyushkov, E. V., On isostatic equilibrium of the earth's crust, *Geophys. J. Roy. Astron. Soc.*, 14, 251, 1967.
- Artyushkov, E. V., Rheological properties of the crust and upper mantle according to data on isostatic movements, *J. Geophys. Res.*, 76, 1376, 1971.
- Berg, C. A., The diffusion of boundary disturbances through a non-Newtonian fluid, in *The Application of Modern Physics to Earth and Planetary Interiors*, edited by S. K. Runcorn, p. 253, Interscience, New York, 1969.
- Birch, F., Elasticity and constitution of the earth's interior, *J. Geophys. Res.*, 57, 227, 1952.
- Bullard, E. C., Heat flow through the floor of the north Pacific ocean, *Nature*, 170, 202, 1952.
- Bullard, E. C., J. E. Everett, and A. G. Smith, Fit of the continents around the Atlantic, *Phil. Trans. Roy. Soc. London, Ser. A*, 258, 41, 1965.
- Buneman, O., A Compact Non-Iterative Poisson Solver, *SUIPR Rep.* 294, 11 pp., Inst. for Plasma Res., Stanford Univ., Stanford, Calif., 1969.
- Busse, F. H., The stability of finite amplitude cellular convection and its relation to an extremum principle, *J. Fluid Mech.*, 30, 625, 1967.
- Busse, F. H., and G. Schubert, Convection in a fluid with two phases, *J. Fluid Mech.*, 48, 801, 1971.
- Chandrasekhar, S., *Hydrodynamic and Hydromagnetic Stability*, 652 pp., Clarendon, Oxford, England, 1961.
- Crittenden, M. D., Effective viscosity of the earth derived from isostatic loading of Pleistocene Lake Bonneville, *J. Geophys. Res.*, 68, 5517, 1963.
- Dicke, R. H., The secular acceleration of the earth's rotation, in *The Earth-Moon System*, edited by B. G. Marsden and A. G. W. Cameron, p. 98, Plenum, New York, 1966.
- Dicke, R. H., Average acceleration of the earth's rotation and the viscosity of the deep mantle, *J. Geophys. Res.*, 74, 5895, 1969.

- Dufort, E. C., and S. P. Frankel, Stability conditions in the numerical treatment of parabolic differential equations, *Math. Tables Other Aids Comput.*, 7, 135, 1953.
- Elsasser, W. M., Early history of the earth, in *Earth Science and Meteoritics*, edited by J. Geiss and E. D. Goldberg, p. 1, North-Holland, Amsterdam, 1963.
- Goldreich, P., and A. Toomre, Some remarks on polar wandering, *J. Geophys. Res.*, 74, 2555, 1969.
- Haskell, N. A., The motion of a viscous fluid under a surface load, 1, *Physics*, 6, 265, 1935.
- Haskell, N. A., The motion of a viscous fluid under a surface load, 2, *Physics*, 7, 56, 1936.
- Heirtzler, J. R., G. O. Dickson, E. M. Herron, W. C. Pitman III, and X. Le Pichon, Marine magnetic anomalies, geomagnetic field reversals, and motions of the ocean floor and continents, *J. Geophys. Res.*, 73, 2119, 1968.
- Holmes, A., Radioactivity and earth movements, *Trans. Geol. Soc. Glasgow*, 18, 559, 1928.
- Horai, K., and S. Uyeda, Terrestrial heat flow in volcanic areas, in *The Earth's Crust and Upper Mantle, Geophys. Monogr. Ser.*, vol. 13, edited by P. J. Hart, p. 95, AGU, Washington, D.C., 1969.
- Ichiye, T., Continental breakup by nonstationary mantle convection generated with differential heating of the crust, *J. Geophys. Res.*, 76, 1139, 1971.
- Isacks, B., J. Oliver, and L. Sykes, Seismology and the new global tectonics, *J. Geophys. Res.*, 73, 5855, 1968.
- Israeli, M., A fast implicit numerical method for time-dependent viscous flows, *Stud. Appl. Math.*, 49, 327, 1970.
- Jeffreys, H., *The Earth*, 420 pp., Cambridge University Press, New York, 1962.
- Julian, B. R., Regional variations in upper mantle structure beneath North America, Ph.D. thesis, 208 pp., Calif. Inst. of Technol., Pasadena, Calif., 1970.
- Knopoff, L., The convection current hypothesis, *Rev. Geophys. Space Phys.*, 2, 89, 1964.
- Knopoff, L., Thermal convection in the earth's mantle, in *The Earth's Mantle*, edited by T. F. Gaskell, p. 171, Academic, New York, 1967.
- Knopoff, L., Continental drift and convection, in *The Earth's Crust and Upper Mantle, Geophys. Monogr. Ser.*, vol. 13, edited by P. J. Hart, p. 683, AGU, Washington, D.C., 1969.
- Krishnamurti, R., On the transition to turbulent convection, 1, The transition from two- to three-dimensional flow, *J. Fluid Mech.*, 42, 295, 1970a.
- Krishnamurti, R., On the transition to turbulent convection, 2, The transition to time-dependent flow, *J. Fluid Mech.*, 42, 309, 1970b.
- Kuo, H-L., Solution of the non-linear equations of cellular convection and heat transport, *J. Fluid Mech.*, 10, 611, 1961.
- Lee, W. H. K., and S. Uyeda, Review of heat flow data, in *Terrestrial Heat Flow, Geophys. Monogr. Ser.*, vol. 8, edited by W. H. K. Lee, p. 87, AGU, Washington, D.C., 1965.
- Le Pichon, X., Sea floor spreading and continental drift, *J. Geophys. Res.*, 73, 3661, 1968.
- MacDonald, G. J. F., The deep structure of continents, *Rev. Geophys.*, 1, 587, 1963.
- MacDonald, G. J. F., The figure and long-term mechanical properties of the earth, in *Advances in Earth Sciences*, edited by P. M. Hurley, p. 199, MIT Press, Cambridge, Mass., 1966.
- Malkus, W. V. R., and G. Veronis, Finite amplitude cellular convection, *J. Fluid Mech.*, 4, 225, 1958.
- McConnell, R. K., Isostatic adjustments in a layered earth, *J. Geophys. Res.*, 70, 5171, 1965.
- McConnell, R. K., Viscosity of the mantle from relaxation time spectra of isostatic adjustment, *J. Geophys. Res.*, 73, 7089, 1968.
- McKenzie, D. P., The influence of boundary conditions and rotation on convection in the earth's mantle, *Geophys. J. Roy. Astron. Soc.*, 15, 457, 1968.
- McKenzie, D. P., Speculations on the consequences and causes of plate motions, *Geophys. J. Roy. Astron. Soc.*, 18, 1, 1969.
- Minear, J. W., and M. N. Toksöz, Thermal regime of a downgoing slab and the new global tectonics, *J. Geophys. Res.*, 75, 1397, 1970.

- Munk, W. H., and G. J. F. MacDonald, *The Rotation of the Earth*, 323 pp., Cambridge University Press, New York, 1960a.
- Munk, W. H., and G. J. F. MacDonald, Continentality and the gravitational field of the earth, *J. Geophys. Res.*, 65, 2169, 1960b.
- Newell, A. C., and J. A. Whitehead, Finite bandwidth, finite amplitude convection, *J. Fluid Mech.*, 38, 279, 1969.
- O'Connell, R. J., Pleistocene glaciation and the viscosity of the lower mantle, *Geophys. J. Roy. Astron. Soc.*, 23, 299, 1971.
- Oliver, J., and B. Isacks, Deep earthquake zones, anomalous structures in the upper mantle, and the lithosphere, *J. Geophys. Res.*, 72, 4259, 1967.
- Orowan, E., Convection in a non-Newtonian mantle, continental drift and mountain building, *Phil. Trans. Roy. Soc. London, Ser. A*, 258, 284, 1965.
- Palm, E., On the tendency towards hexagonal cells in steady convection, *J. Fluid Mech.*, 8, 183, 1960.
- Pan, F., and A. Acrivos, Steady flow in rectangular cavities, *J. Fluid Mech.*, 28, 643, 1967.
- Rayleigh, Lord (J. W. Strutt), On convection currents in a horizontal layer of fluid when the higher temperature is on the under side, *Phil. Mag., Ser. 6*, 32, 529, 1916.
- Ringwood, A. E., Phase transformations and mantle dynamics, *Earth Planet. Sci. Lett.*, 14, 233, 1972.
- Roberts, P. H., Convection in horizontal layers with internal heat generation, Theory, *J. Fluid Mech.*, 30, 33, 1967.
- Runcorn, S. K., Convection in the mantle, in *The Earth's Crust and Upper Mantle*, *Geophys. Monogr. Ser.*, vol. 13, edited by P. J. Hart, p. 692, AGU, Washington, D.C., 1969.
- Schatz, J. F., and G. Simmons, Thermal conductivity of earth materials at high temperatures, *J. Geophys. Res.*, 77, 6966, 1972.
- Schubert, G., and D. L. Turcotte, Phase changes and mantle convection, *J. Geophys. Res.*, 76, 1424, 1971.
- Sclater, J. G., and J. Francheteau, The implications of terrestrial heat flow observations on current tectonic and geochemical models of the crust and upper mantle of the earth, *Geophys. J. Roy. Astron. Soc.*, 20, 493, 1970.
- Segel, L. A., Distant side walls cause slow amplitude modulation of cellular convection, *J. Fluid Mech.*, 38, 203, 1969.
- Simmons, G., and R. F. Roy, Heat flow in North America, in *The Earth's Crust and Upper Mantle*, *Geophys. Monogr. Ser.*, vol. 13, edited by P. J. Hart, p. 78, AGU, Washington, D.C., 1969.
- Sykes, L. R., Mechanisms of earthquakes and nature of faulting on the mid-ocean ridges, *J. Geophys. Res.*, 72, 2131, 1967.
- Thirlby, R., Convection in an internally heated layer, *J. Fluid Mech.*, 44, 673, 1970.
- Torrance, K. E., and D. L. Turcotte, Structure of convection cells in the mantle, *J. Geophys. Res.*, 76, 1154, 1971.
- Tritton, D. J., and M. N. Zarraga, Convection in horizontal layers with internal heat generation, Experiments, *J. Fluid Mech.*, 30, 21, 1967.
- Turcotte, D. L., and G. Schubert, Structure of olivine-spinel phase boundary in descending lithosphere, *J. Geophys. Res.*, 76, 7980, 1971.
- Turcotte, D. L., and E. R. Oxburgh, Mantle convection and the new global tectonics, *Annu. Rev. Fluid Mech.*, 4, 33, 1972.
- Verhoogen, J., The adiabatic gradient in the mantle, *Eos Trans. AGU*, 32, 41, 1951.
- Verhoogen, J., Phase changes and convection in the earth's mantle, *Trans. Roy. Soc. London, Ser. A*, 258, 276, 1965.
- Vine, F. J., and D. H. Matthews, Magnetic anomalies over ocean ridges, *Nature*, 199, 947, 1963.
- Von Herzen, R. P., and W. H. K. Lee, Heat flow in oceanic regions, in *The Earth's Crust and Upper Mantle*, *Geophys. Monogr.*, vol. 13, edited by P. J. Hart, p. 88, AGU, Washington, D.C., 1969.

- Weertman, J., The creep strength of the earth's mantle, *Rev. Geophys. Space Phys.*, 8, 145, 1970.
- Wegener, A., *The Origin of Continents and Oceans*, 212 pp., Dutton, New York, 1924.

(Received November 19, 1972; revised January 8, 1973.)